PHILOSOPHICAL TRANSACTIONS OF THE ROYAL SOCIETY B BIOLOGICAL SCIENCES

Diffusion and Binding Measurements within Oral Biofilms Using Fluorescence Photobleaching Recovery Methods

J. J. Birmingham, N. P. Hughes and R. Treloar

Phil. Trans. R. Soc. Lond. B 1995 **350**, 325-343
doi: 10.1098/rstb.1995.0168

Diffusion and binding measurements within oral biofilms using fluorescence photobleaching recovery methods

J. J. BIRMINGHAM, N. P. HUGHES AND R. TRELOAR

Unilever Research Port Sunlight Laboratory, Quarry Road East, Bebington, Wirral L63 3JW, U.K.

SUMMARY

Numerous studies have postulated that bacteria which reside in a biofilm differ from planktonic bacteria. These differences are thought to affect biofilm permeability and, indirectly, the susceptibility of biofilm bacteria to antibacterial agents. In this study fluorescence recovery after photobleaching (FRAP) was used to monitor the diffusion and binding characteristics of a set of size fractionated fluorescein isothiocyanate (FITC)-conjugated dextrans over small areas (ca. 10 μm) in bacterial biofilms. From these measurements it was straightforward to calculate apparent diffusion rates. Initial studies on the concentration dependence of dextran interaction with planktonic bacteria showed that no irreversible interaction was occurring, however, anomalous faster than free solution diffusion rates were obtained. This phenomenon was modelled using novel analytical and numerical methods which incorporate reversible binding with associated fluorescence changes. Apparent diffusion rates measured in biofilms were highly dependent on biofilm preparation. Sucrose starved biofilms produced an apparent slow-down of two- to fivefold depending on dextran molecular mass and location within the biofilm, indicating that diffusion within the biofilm is hindered. Sucrose supplemented biofilms produced apparent diffusion rates close to those in free solution, suggesting less hindered diffusion. *Ex vivo* plaque showed diffusion and binding similar to the sucrose supplemented biofilms. The FRAP approach provides a fast and convenient method for determining diffusion rates over small areas within bacterial biofilms. This study reinforces the importance of considering the influence of reversible binding and associated fluorescence changes, as these may have a marked effect on the measured apparent diffusion rate.

1. INTRODUCTION

It is now well established that bacteria which reside within a biofilm differ in several key respects to planktonic bacteria (Costerton *et al.* 1987, 1994; Geesey *et al.* 1992; Costerton 1994). These differences arise from the specific adhesion events which control biofilm build-up (Kolenbrander 1991), the complex matrices produced by adherent bacteria (Lawrence *et al.* 1991; Cummins *et al.* 1992; Wolfaardt *et al.* 1994) and the subsequent matrix-influenced growth (Capdeville *et al.* 1992). It has been suggested that these differences will have a marked effect on biofilm permeability and any permeability-selective behaviour is likely to effect ecology (Bradshaw *et al.* 1989). Diffusion through dental plaque has specifically been proposed as an important rate-determining factor in decay (Edgar 1989) because dietary sugars must diffuse through the outer layers of plaque to sustain acidogenic bacteria at the tooth surface, and bacterially produced organic acids may have their cariogenicity attenuated by free diffusion from the plaque (Dibdin 1981, 1992). Further, biofilm permeability will effect the penetration of antibacterial agents to their target sites in a bacterial film (Govan 1975; Baltimore & Mitchell 1980; Rueska *et al.* 1982). Some data suggests that extracellular polysaccharide producing bacteria, existing as biofilms, are less susceptible to antibiotics than freely suspended bacteria (Nickel *et al.* 1985, 1988). Moreover, it has been postulated in one case that the extracellular material completely excludes antibacterial agents (Costerton *et al.* 1987).

In several studies agents have been introduced to biofilms, and their diffusion has been traced directly over time (using radiolabels, microelectrodes etc.), usually in concert with a suitable measure of the activity of the agent for example, zone of inhibition (Nichols *et al.* 1988). This is an extremely direct way of measuring diffusion, however it requires large plaque samples which can be grown reproducibly. In general this means that these studies have been performed on single species plaques. Alternatively biofilms have been harvested from human volunteers and pooled to produce a single homogenized bacterial clump. Again the diffusion rate of a radiolabelled agent is tracked through this bacterial clump (Dibdin 1981; McNee *et al.* 1982; Tatevossian 1985). To probe the permeability of biofilms extensively fluorescence recovery after photobleaching (FRAP) of a series of fluorescently conjugated dextrans of differing molecular masses was carried out in this study. This approach is a convenient and quick method capable of measuring diffusion rates

Phil. Trans. R. Soc. Lond. B (1995) **350**, 325–343
Printed in Great Britain

over small areas within a sample (Thomas & Webb 1990). In brief the technique involves: (i) introducing a fluorescent probe reporter molecule which is allowed to freely diffuse through the system to create a homogenous distribution; (ii) create a fluorescence gradient by photobleaching a fixed volume of the probe; and (iii) track the rate of fluorescence redistribution and calculate a diffusion rate. It is important at the outset to appreciate that FRAP reports on all of the motion of a fluorescently tagged macromolecule within a particular environment. Thus if the molecule is irreversibly bound within the environment then the subsequent recovery will be suitably attenuated. Equally if the molecule is reversibly binding within the environment this factor needs to be considered in the interpretation of the recovery.

Previous work using dextrans as a permeability probe for biofilms established that no irreversible probe binding was occurring (Lawrence *et al.* 1994). However, this work overlooked the possibility of reversible probe binding. To check for reversible binding, an initial set of experiments was carried out in this study in which a single dextran was titrated against fixed bacterial concentrations. These data were then modelled using novel analytical and numerical approaches for the interaction of a mobile fluorescent macromolecule with an immobile bacterial matrix to produce transient fluorescent complexes. Subsequently FRAP was used to obtain effective diffusion rates of dextrans within unperturbed mixed-species *in vitro* biofilms and *ex vivo* oral plaques.

2. EXPERIMENTAL

(a) *Bacterial suspensions and biofilm growth*

Suspensions of *Streptococcus oralis* 209 were grown in a brain-heart infusion (BHI) broth. They were then washed extensively in phosphate buffered saline (pH 6.5) before use. Mixed species *in vitro* biofilms were prepared from a defined mixed culture of ten oral bacteria (*Streptococcus mutans* R9, *Streptococcus gordonii* NCTC 7865, *Streptococcus oralis* EF 186, *Actinomyces viscosus* WVU 627, *Lactobacillus casei* AC 413, *Neisseria subflava* A 1078, *Veillonella dispar* ATCC 17745, *Prevotella intermedia* T 588, *Porphyromonas gingivalis* W 50 and *Fusobacterium nucleatum* ATCC 10953). The biofilm was produced in a specially designed chemostat fermenter and the general protocol used is described in full by Bradshaw *et al.* (1989). In this particular instance the biofilms were grown on 7 mm square glass tiles for 5 days in the chemostat, rather than the more normal hydroxyapatite tiles. This change made imaging of the biofilms much more straightforward, allowing the laser to be focussed fully in the biofilm for FRAP measurements. Thick biofilms were produced after 5 days. These biofilms have been extensively studied (Bradshaw *et al.* 1989). The initial films have been shown as reproducible in terms of microbiological composition and cariogenic pulse experiments have shown increases in *S. mutans* and *L. casei* (Bradshaw *et al.* 1992). On removal from the chemostat, half of the biofilms were maintained in growth medium (0.25% sucrose w/w, termed sucrose starved), whereas the others were placed in sucrose supplemented growth medium (5% sucrose w/w) overnight. Immediately before preparation for FRAP measurements the biofilms were removed from growth medium and bathed in phosphate buffered saline for ca. 30 mins.

Oral plaques were grown on a tile of roughened plastic placed in a denture insert which was worn by a human subject for 24 h. A similar method has previously been used to insert enamel slabs into human subjects for re/demineralisation studies (Schafer 1989). To encourage bacterial colonization, the tile was dosed with ca. 1 ml of a 5% sucrose solution every 5 h. After 24 h a thick bacterial film was visible to the naked eye. The subject ate normally throughout the 24 h but refrained from any oral hygiene. Before FRAP measurements the tile was carefully removed from the insert, ensuring that the bacterial film was not perturbed and bathed in phosphate buffered saline as above.

(b) *FRAP sample preparation*

The single bacterial strain used for planktonic experiments was *S. oralis* 209 and a single 40 kDa dextran type was chosen as a typical macromolecular diffusant. Two bacterial densities were employed to illustrate the extremes possible: low and high, where 'high' was 50 times the concentration of 'low'. The approximate bacterial densities (total count) were 10^7 per ml (low) and 5×10^8 per ml (high). The concentration range for the 40 kDa dextran spanned 0.1–10 μM, where the concentration refers to fluorescein isothiocyanate (FITC) concentration, not dextran or glucose residue concentration.

The bacterial films were doped with FITC-labelled dextrans covering a wide molecular mass range (Sigma FD-10, FD-40, FD-500) to achieve a final FITC label concentration of 10 μM. Typically 100 μl of the dextran stocks were directly added to an O-ring supported, inverted film substrate in buffer medium, so that the biofilm faced towards the large cover-slip of a Bionique chamber dish without fear of crushing. The chamber was covered with a watch-glass and incubated at room temperature for 30 mins.

(c) *Fluorescence recovery apparatus*

The FRAP apparatus used is shown schematically in figure 1. It is a custom-built laser/microscope combination designed to provide good detection sensitivity and speed rather than conventional fluorescence microscopy imaging. An air-cooled Lexel-65 Ar-ion laser beam, (30 mW max at 488.0 nm in Light Control Mode, 10–15 mW typical this work) is focussed onto the entrance port of a purpose-built inverted fluorescence microscope. Intensity control of the laser beam is achieved via an acousto-optic modulator (AOM Coherent model 304D), which generates either brief (10 μs) probe pulses or a single stretched pulse to enable bleaching. This allows a single-beam FRAP configuration via pulse duty-cycle manipulation as described by Garland (1981). The laser-beam is optimally reflected up towards the sample by a dichroic mirror and focussed using an Olympus MSPlan ×50

PHILOSOPHICAL TRANSACTIONS OF THE ROYAL SOCIETY B BIOLOGICAL SCIENCES

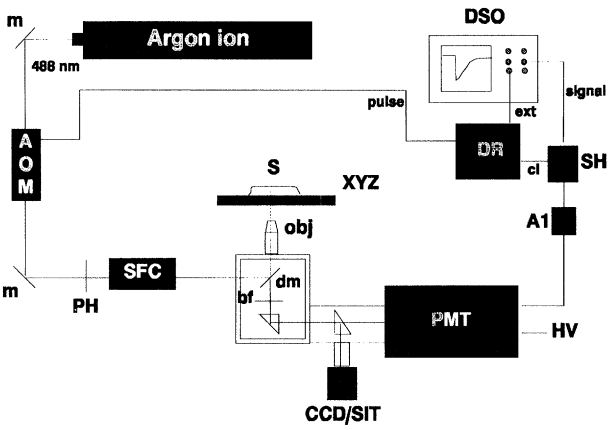

Figure 1. FRAP instrument layout: symbols denote the following components. M coupling mirrors; AOM acousto-optic modulator; PH first order isolation pinhole; SFC collimating spatial filter; S sample contained on XYZ stage and excited/imaged via microscope objective OBJ; DM dichroic mirror; BF barrier filter; CCD slow-scan charge coupled device camera (beamsizing); SIT video-rate Silicon Intensified Target camera (general viewing); PMT Photo-Multiplier Tube, fed with high voltage HV; A1 trans-impedance preamplifier; SH sample-and-hold amplifier; DR driver electronics; DSO digital storage oscilloscope.

ULWD objective with a numerical aperture (NA) of 0.55. The sample is contained typically in a Bionique Labs CD-100 sample chamber, mounted on a purpose-built thermostatted stage assembly. The FRAP detector is a Thorn-EMI 9863B/350 photomultiplier tube cooled to −25 °C (PMT, 14-stage fast photon-counting S20 type) whereas the standard imaging detector is a Silicon Intensified Target (SIT) video-camera (JAI 732). A B/W video-image viewed on a Panasonic video monitor is used to focus the FRAP laser spot on to areas of interest in the sample. Such areas were chosen randomly and where distinct differences were observed in bacterial density across a sample, measurements were taken across a representative spread of densities. When quantitative beam-sizing is required, the fluorescence spot image is let fall on a cooled slow-scan charged coupled device (CCD) camera (AT1 Wrights Instruments system).

The FRAP experiment is almost entirely run from Hewlett Packard software which sets up the beam duty-cycle parameters as well as performing the whole experimental sequence. Repeat-bleaching of fully recovering samples is catered for in addition to the standard single-shot FRAP experiment. Nonlinear least-squares curve fitting of such averaged traces is carried out to a 2-D diffusion model (see §2*d*). Beam sizing of the CCD laser-spot images acquired under non-bleaching conditions is performed external to the AT1 commercial software in a HP-emulation environment called HTBasic.

FRAP measurements were taken at several separate locations in repeated bleach mode. Fluorescence beam images were always taken at each location visited without altering in any way the focus situation that pertained during the FRAP run. Pure solution runs or experiments involving non-biofilm planktonic suspensions did not require multiple locations, but care was taken to allow such samples to completely settle before performing the diffusion measurements so as to minimize the contribution of flow to the measured fluorescence recovery.

(*d*) FRAP *data analysis*

All FRAP recovery traces were fitted using standard two-dimensional (2-D) diffusion models for a Gaussian laser beam profile assuming an infinite homogeneous pool of label exists external to the laser spot. Allowance is also made for immobile fractions. The general fitting equation is then of the form:

$$F(t)/F_0 = Rf(f(t)) + (1 - Rf),$$

where $F(t)$ denotes the measured fluorescence intensity at post-bleach time t, F_0 denotes the initial prebleach intensity, and Rf denotes the mobile fraction defined as:

$$Rf = (F(\infty) - F(0))/(F_0 - F(0)).$$

For pure diffusion, $f(t)$ is as given by Axelrod *et al.* (1976):

$$f(t) = \sum_{n=0}^{\infty} \frac{(-\kappa)^n}{n!} \frac{1}{[1 + n(1 + (2t/\tau_d))]},$$

where κ is the sample bleach constant and where τ_d is the 2-D characteristic diffusion time:

$$\tau_d = w^2/4D_L$$

with ω the e^{-2} laser beam radius for both the bleaching and monitoring phases of the FRAP experiment and D_L the sample lateral diffusion coefficient.

The algorithm of choice for fitting such models to the experimental data is that of Marquardt nonlinear least-squares (Marquardt 1963), following the basic code given by Bevington (1969). Explicit partial derivatives with respect to the fitting parameters were used in all cases, with usually 16 terms of the Axelrod $F(t)$ summation used. The model parameters estimated by this procedure are:

$$\kappa,\ \tau_d,\ F(\infty)/F_0,$$

along with the estimated parameter standard deviations. The latter will be meaningful only if an averaged FRAP trace is being fitted, as in this case channel-by-channel signal variances are available from the averaging program to reciprocally weight the fitting process. The laser beam fitting procedure also uses the Marquardt fitting algorithm with reciprocal weighting on the CCD pixel counts (Poissonian counting statistics) to estimate the e^{-2} radii of the central horizontal and vertical sections. The fitting model assumes a gaussian profile superimposed on an arbitrary quadratic polynomial background. The e^{-2} radii of the two central slices are then averaged to a single value before calculating D_L.

Values for %-recoveries $(100 \times Rf)$ significantly different from 100 % denote immobile fractions on the timescale of the FRAP experiment. Repeated bleaches on such samples are not expected to yield similar-form recoveries with each bleach. This is because the truly immobile fraction is being gradually removed from the fluorescence signal, as it is being repeatedly bleached without a mechanism for replacement by unbleached

PHILOSOPHICAL TRANSACTIONS OF THE ROYAL SOCIETY B BIOLOGICAL SCIENCES

label from the external pool. This implies that the percentage-recovery will gradually approach 100% with repeated bleaching in such instances, as the signal will eventually consist of just the mobile, exchangeable species.

Reversible binding could also alter the apparent diffusion times without giving any evidence of a clearly immobile fraction. Section 3*b* below summarizes the development of some novel FRAP equations covering simple reversible bimolecular reactions combined with diffusion of both partners, either with or without fluorescence changes upon binding.

The effect of diffusional recovery along the microscope axis on the otherwise radial FRAP recovery depends strongly on the relative characteristic distances of the laser beam along these two directions. Even for deep bleaches, the worst-case situation would be that the measured diffusion coefficients should be halved if the beam characteristic distances are equal (J. J. Birmingham, unpublished data). Because relatively low NA objectives and no deliberate detector aperturing have been employed in this work, it is unlikely that a significant three-dimensional (3-D) correction is warranted in this case.

Fractional rather than normalized FRAP recovery functions are used in this study for display purposes. The fractional recovery function is defined as:

$$Fr(t) = (F(t) - F(0)) - (F(\infty) - F(0)),$$

where $F(t)$ denotes raw fluorescence signal at time t and $f(t)$ denotes the theoretically derived normalized recovery function already used above:

$$f(t) = F(t)/F_0.$$

Specifically this allows the graphical comparison of a set of FRAP recovery functions even though they may have different bleach depths. The fractional FRAP form always has the standard (0,1) range unlike the parent $f(t)$ form.

(*e*) *Microscopy*

Differential interference contrast (DIC) optical microscopy was performed on both *in vitro* and *ex vivo* biofilms using an Olympus BH2 microscope. Images were obtained on Ilford FP4–125ISA film. Low temperature scanning electron microscopy was performed on sucrose treated *in vitro* biofilms. This technique involves plunging the specimen under vacuum into nitrogen slush at −192 °C. Such rapid cooling helps to retain biofilm integrity (Sutton *et al.* 1994). The specimen was then lightly etched to remove any traces of surface ice and gold coated prior to examination in a Cambridge S120 scanning electron microscope. Images were obtained on Kodak PLUS-XPAN film.

3. EFFECTIVE DIFFUSION RATES MEASURED IN PLANKTONIC BACTERIA

(*a*) *Results*

Table 1 details 14 experiments, each experiment the result of averaging 20 individual FRAP traces. The first row in each experiment is the mean parameter value, the second row is the estimated standard deviation (in brackets). In table 1 low and high bacterial densities are indicated, beam denotes the average e^{-2} non-bleaching laser beam radius and T_{bl} is the experimental bleach time (ms). For experiments 9*a* onwards, it was necessary to increase T_{bl}. The fitted κ-values in these experiments were scaled by the increase in bleach time so as to calculate an effective %-bleach as if the 'standard' 40 ms bleach time were used. This allows a comparison of %-bleach across the concentration range in the high bacterial density case. In all cases bleach recovery was complete (at least 95%).

Experiment 1 is the bacteria-free control, giving a diffusion coefficient just below 10^{-6} cm^2 s^{-1}. The low bacterial density experiments (2–6) show similar diffusion coefficients, with little or no trend as a function of dextran concentration apparent. The high bacterial density experiments (7–10) are, however, very different. The effective laser beam radius broadens somewhat, reflecting significant bacterial packing and hence scattering (this effect is more marked for the biofilm experiments, see §4*a*). Each dextran concentration was repeated in a second location in these high density experiments (*a*, *b*), as slightly different bacterial packing could be possible at different sampling points. As the dextran concentration is lowered, the %-bleach falls drastically (hence the necessity of T_{bl} adjustment). The D_L values show a very significant increase in apparent diffusional exchange rate compared to bacteria-free control or to the low density cases. Values 'closer' to the expected free solution value occur at either end of the concentration range tested, but intermediate cases give the largest increase in apparent D_L. The 40 kDa dextran molecule appears to be moving some four times faster in the dense bacteria case with an apparent concentration optimum for this effect, whilst the inherent bleachability of the label falls steadily as the total concentration of diffusant falls. As FRAP is a relative fluorescence measurement, all data being normalized by the prebleach fluorescence level, we cannot however say anything about the inherent fluorescence efficiencies across the concentration range.

(*b*) *Discussion*

The measured apparent diffusion rates would have been naively expected to show modest retardation effects with little or no concentration dependence if no interaction was occurring between the bacteria and the dextran probe, and all that was occurring was a slight reduction in effective viscosity of the 'solutions'. Viscosities were not in fact measured for these samples but we expect the D_L values quoted to be further increased if such viscosity effects were taken into account for the high bacterial density set, relative to the bacteria-free control.

The reduction in bleach efficiency seems to indicate a dextran-bacterial interaction of some sort, provided overall dissolved oxygen levels are not somehow being affected. Photobleaching requires molecular oxygen, so is it possible that the trend in %-bleach follows dissolved oxygen levels, taking elapsed time between start of incubation and actual measurement into

PHILOSOPHICAL TRANSACTIONS OF THE ROYAL SOCIETY B BIOLOGICAL SCIENCES

Table 1. *Planktonic diffusion results*

(Low and high refer to bacterial concentrations (§2*b*). Figures in brackets are standard deviations.)

	dye	beam	T_{b1}			$D_L \times 10^6$
expt	μM	μM	ms	% bleach	eff-% bleach	$cm^2\ s^{-1}$
1	10	9.64 (0.07)	40	62.71 (0.06)	–	0.7404 (0.0113)
2	low 10	9.96 (0.07)	40	60.88 (0.10)	–	0.8738 (0.0121)
3	low 5	9.56 (0.07)	40	59.67 (0.10)	–	0.8339 (0.0133)
4	low 1	9.59 (0.07)	40	48.97 (0.12)	–	0.5882 (0.0098)
5	low 0.5	10.15 (0.07)	40	57.83 (0.19)	–	0.9337 (0.0148)
6	low 0.1	10.47 (0.10)	40	49.43 (0.29)	–	0.7769 (0.0208)
7*a*	high 5	12.05 (0.14)	40	42.56 (0.09)	–	1.3520 (0.0335)
7*b*	high 5	12.05 (0.15)	40	40.46 (0.12)	–	1.8112 (0.0479)
8*a*	high 1	10.41 (0.09)	40	25.79 (0.20)	–	3.2487 (0.0792)
8*b*	high 1	11.41 (0.08)	40	20.77 (0.33)	–	3.7761 (0.1236)
9*a*	high 0.5	12.05 (0.12)	80	21.29 (0.24)	11.51	2.2345 (0.0745)
9*b*	high 0.5	11.18 (0.11)	120	18.77 (0.24)	6.85	1.4893 (0.0539)
10*a*	high 0.1	11.13 (0.09)	120	21.43 (0.35)	7.94	1.6455 (0.0677)
10*b*	high 0.1	11.53 (0.12)	120	22.56 (0.31)	8.41	1.6621 (0.0612)

account? Careful examination of the experimental sequence and times, together with Clark-oxygen electrode measurements taken with or without 40 kDa dextran appear to rule out this possibility (N. P. Hughes & J. J. Birmingham, unpublished results). The planktonic bacteria used were washed carefully to exclude detritus and possible nutrients before any FRAP measurements. The overall oxygen consumption rates as determined by standard oxygen electrode methods were very low indeed, with no evidence that dextran concentrations as used in the experiments above could induce any increase in this low basal rate. Deliberately added sucrose did however stimulate oxygen uptake as expected, indicating that the samples were potentially metabolically active under the right conditions. Thus the 40 kDa dextran does not act as a nutrient source for oxidative metabolism, and the samples are clean enough to ensure minimal oxygen level decreases over the periods of time used in the FRAP experiments. We therefore conclude that the reduction in bleach efficiency indicates a direct dextran-bacterial interaction. Because the %-recoveries are always very close to 100%, this cannot be a permanent or irreversible association between the dextran and the bacterial surface.

The interaction must be reversible or transient on the timescales of the FRAP experiments and sufficient to provide very significant bleach protection when the FITC-dextran is surface-associated. The bacteria although not absolutely static in these experiments are obviously very much less mobile than the dextran, so if the association were not reversible we should have seen a significant lack of recovery or very slow components. The data of course show marked enhancement in apparent diffusion rates, not reductions. The challenge then is to model a reversibly interacting system as regards FRAP-signals, allowing for large changes in inherent bleachability and possibly also in fluorescence yields between the 'free' and 'bound' fluorescent states. This amounts to a two-component coupled reaction/diffusion system. Both analytic and numerical models of such a system are presented below.

(i) *Reversible binding FRAP effects: analytic approach*

Conventional FRAP deals with binding phenomena only indirectly via the measurement of immobile fractions generated by irreversible binding to a stationary substrate. The term irreversible denotes no significant desorption during the timescale of the FRAP experiment in question. The equations derived below deal with the domain of problems usually identified with the technique known as fluorescence correlation spectroscopy (FCS), i.e. combined diffusion and reaction chemistry. Very few of the same models have ever been worked through in a FRAP context, although the two techniques have a lot in common. FCS measures diffusion and chemical kinetic rates by measuring the systematic component of the fluctuating fluorescence

PHILOSOPHICAL TRANSACTIONS OF THE ROYAL SOCIETY B BIOLOGICAL SCIENCES

signal as a fluorescently tagged molecule diffuses and/or reacts with other species in a small defined volume of a sample. The measure of choice is usually the autocorrelation function, which decays in time at a rate determined by the diffusion and reaction timescales of the sample. FCS was developed historically earlier than FRAP (Magde *et al.* 1972, 1974; Elson & Magde 1974; Aragon & Pecora 1975; Ehrenberg & Rigler 1976), but was not widely pursued subsequently due to a variety of practical problems with the technique. The principal problem was the very long acquisition times, which led to substantial photobleaching artifacts, as well as problematic laser fluctuations with correlation times not very different from those of the sample's kinetics. Some of the FCS pioneers then developed the FRAP method, which was seen as especially suitable for the growing area of cell biology membrane dynamics (Peters *et al.* 1974; Axelrod *et al.* 1976). The FRAP method gave data on an experimentally convenient timescale, and could measure microscopically local data on interesting biological systems. FCS thus fell by the wayside with FRAP filling its niche almost completely. However, there has been a very recent resurgence in FCS methods (Meyer & Schindler 1988; Rigler *et al.* 1993*a*, *b*; Mets & Rigler 1994; Widengren *et al.* 1994), driven by confocal geometry and detector/correlator improvements. The generation of ultra-small confocal detection volumes results in characteristic diffusion times very much faster than in classic-FCS, thus avoiding problematic fluctuation timescales of the apparatus itself, as well as radically shortening the total acquisition times. We can anticipate that FCS will re-emerge as a useful tool, especially in the area of coupled reaction and diffusion in the next few years.

Only one specific example of a FRAP recovery function allowing for some form of binding together with diffusion (and flow) appears to have been given before (Elson 1986) although general comments on what such FRAP recovery functions should contain have been stated (Elson 1985). The specific example given by Elson (1986) details a unimolecular isomerization between two fluorescent states, which are however assumed to have equal diffusion coefficients, but generally unequal bleaching kinetics and emission quantum yields. The experimental situation in this study does not match Elson's model: we require a reversible bimolecular reaction scheme (labelled dextran onto bacterial plaque binding sites) where the lateral diffusion of the two partners are certainly very different. It is also perfectly possible that both the bleaching characteristics and fluorescence emission yields could be quantitatively different in the bound and free states for our application. For these reasons we have derived the theoretical FRAP recovery functions de novo, allowing for differential diffusion of the reaction partners along with differential bleaching and emission properties.

Here we will consider the simple bimolecular reaction:

$$A + B \Leftrightarrow C,$$

where A in this context denotes non-fluorescent bacterial surface dextran binding sites, B denotes free labelled dextran and C denotes the transient complex (also fluorescent). Both fluorescent partners (B and C) are allowed to diffuse in a radially symmetric 2-D manner. Importantly, these reaction species are assumed to be homogeneously distributed both within the monitoring beam and in the external pool. Thus no spatial extent or geometry for the bacterial partner (A-C) is allowed for: the situation to be tractable analytically is imagined to be modellable as a solution in which reversible binding or reaction is occurring in addition to free diffusion of all the species.

Species A is taken to be non-fluorescent, whereas B and C will obviously be fluorescent. Therefore the concentration of A will not have a FRAP evolution equation unlike the species B and C. It is generally supposed that the reversible reaction of B with A to form C is at equilibrium before the photobleach event. Thus we will have two FRAP evolution equations, one each for B and C, in which only the equilibrium concentration of species A can appear. The photobleaching process cannot affect a non-fluorescent species, so its dynamic concentration cannot alter from its equilibrium value as the fluorescent species redistribute with post-bleach time. The bimolecular reaction scheme and the two evolution equations are:

$$A + B \Leftrightarrow C \quad K_{eq} = k_f/k_b = C_c^{eq}/(C_a^{eq} C_b^{eq})$$

$$\partial C_b/\partial t = D_b \nabla^2 C_b - k_f C_a^{eq} C_b + k_b C_c$$

$$\partial C_c/\partial t = D_c \nabla^2 C_c - k_b C_c + k_f C_a^{eq} C_b$$

The reaction is characterized by an equilibrium constant K_{eq} given by the ratio of the forward k_f and the backward k_b rate constants or given by the usual ratio of equilibrium concentrations of the species. We need to solve for the dynamic concentrations of the fluorescent species B and C post-bleach, which will also be spatially dependent due to the spatial aspects of the laser beam. Only the standard 2-D-radial FRAP spot geometry case will be covered here, so the Laplacian operator will be:

$$\nabla^2 = \frac{1\partial}{r\partial r}\left(r\frac{\partial}{\partial r}\right).$$

The explicit solution route to this coupled reaction/diffusion system will not be given here but the principal steps include the following. After switching to bleached diffusant variables, the partial differential equation system is reduced to an ordinary differential equation system by Hankel transformation (circularly symmetric 2-D Fourier transformation, see Bracewell 1986). The general solution to this ordinary system is then easily derived by standard matrix methods, see Hurewicz (1975). Proceeding as in former FCS work (Elson & Magde 1974), it is then assumed that the system is in the diffusion limit, an assumption which allows considerable simplification of the eigenvalues and pre-exponential weightings. The FRAP normalized fluorescence recovery signal is derived from this simplified system solution by Hankel inversion and weighted integration steps. The latter step explicitly takes the differential quantum yields for free and bound ligand into account. Differential bleaching sensitivities for the

PHILOSOPHICAL TRANSACTIONS OF THE ROYAL SOCIETY B BIOLOGICAL SCIENCES

fluorophore in the free and bound states are included via the initial conditions for the transient concentrations of B and C, just as in standard pure diffusion FRAP (Axelrod *et al.* 1976).

This diffusion-limit assumption is explicitly:

$$R = k_f C_a^{eq} + k_b >> 4(D_b - D_c)/\omega^2,$$

where k_f and k_b denote the forward and backward rate constants respectively, C_a^{eq} denotes the equilibrium concentration of free binding sites, ω denotes the e^{-2} radius of the laser beam (both monitoring and bleaching) and R denotes the overall chemical relaxation rate constant. In our case we can take the diffusion coefficient of the bacteria to be negligible (D_c zero) so this assumption refers to the relative scaling of the diffusion of the free dextran to the binding/unbinding rates. For example, a 40 kDa dextran with a D_b of say 10^{-6} cm^2 s^{-1} and a beam radius of 10 μm, gives a characteristic diffusion time of 250 ms or a diffusional rate of 4 s^{-1} across the interrogated region. For the final equation to hold, the chemical exchange rate should be at least as fast as this, and preferably considerably larger.

The final complete expression for the normalised FRAP signal turns out to be the following complex expression:

$$\frac{F(t)}{F_0} = 1 + \sum_{n=1}^{\infty} \frac{[\phi_b(-\kappa_b)^n + \phi_c(-\kappa_c)^n]}{n![1+n(1+2t((\phi_b/\tau_b)+(\phi_c/\tau_c)))]}$$

$$- \left\{ \frac{2\phi_b\phi_c}{R} \times \left(\frac{1}{\tau_b} - \frac{1}{\tau_c}\right) \sum_{n=1}^{\infty} \frac{[(1+\phi_b\epsilon)(-\kappa_b)^n - (1-\phi_c\epsilon)(-\kappa_c)^n]}{(n-1)!} \right.$$

$$\left. \times \left(\frac{1}{[1+n(1+2t((\phi_b/\tau_b)+(\phi_c/\tau_c)))]^2} - \frac{\exp(-Rt)}{[1+n(1+2t((\phi_c/\tau_b)+(\phi_b/\tau_c)))]^2} \right) \right\}$$

$$+ \left(\phi_b\phi_c\epsilon\exp(-Rt) \times \sum_{n=1}^{\infty} \frac{[(-\kappa_b)^n - (-\kappa_c)^n]}{n![1+n(1+2t((\phi_c/\tau_b)+(\phi_b/\tau_c)))]} \right).$$

The symbols are defined as follows:

$$\tau_b = \omega^2/4D_b \qquad \tau_c = \omega^2/4D_c$$

$$\phi_b = C_b^{eq}/C_t \qquad \phi_c = C_c^{eq}/C_t$$

$$\epsilon = (\eta_b - \eta_c)/\eta_b\phi_b + \eta_c\phi_c)$$

The free ligand B has a bleach constant κ_b, a free fraction at equilibrium of ϕ_b (C_t is the total labelled ligand concentration), a characteristic diffusion time of τ_b and a fluorescence quantum yield of η_b. The corresponding quantities for the complex C are labelled similarly, with ϕ_c now denoting the bound fraction at equilibrium. The sum of these two fractions of course equals one. The term ϵ is essentially a normalized quantum yield difference. Compare the complexity of this expression with the standard pure diffusion FRAP result, denoted $f(t)$ in §2*d*. The complex expression trivially includes the standard result if there is no binding reaction (put bound fraction to zero). Like the earlier $f(t)$ result, the long-term time behaviour implied by this complex expression is that of complete recovery.

Several special cases of this equation may be considered.

1. If there are no bleaching or quantum yield differences to let FRAP distinguish between states B and C, then the only effect of transient binding is to generate a FRAP recovery function of identical form to the classic pure diffusional form, but with an effective diffusion coefficient:

$$D_{eff} = \phi_b D_b + \phi_c D_c.$$

Thus if the diffusion of the complex is much slower than that of the free ligand, the measured diffusion coefficient can vary anywhere between D_c (lower limit) and the 'true' value D_b (upper limit). The effect is thus always one of effective retardation.

2. If only one of the fluorescence parameters differ between states B and C (i.e. bleach constant or quantum yield but not both), then the overall qualitative effect is also one of effective retardation. There are quantitative differences in the apparent rates of recovery relative to the first case above, but apparent diffusion coefficients appear to never exceed the true free-ligand value.

3. If there are differences in both fluorescence parameters (quantum yield and bleach constant) between states B and C, then a remarkable range of phenomena can result. A useful illustration of this can be obtained by considering the extreme case of full photobleaching protection and full fluorescence quenching in the bound state, where it is also assumed that the complex is diffusionally immobile. Taking formal limits of the resultant general expression as the fraction of free ligand approaches zero or one, we will obtain in this case:

1. low total ligand limit: $\phi_b \to 0$, $\phi_c \to 1$,

$$Lim\left(\frac{F(t)}{F_0} - 1\right) = \exp(-Rt) \sum_{n=1}^{\infty} \frac{(-\kappa_b)^n}{n![1+n(1+2t/\tau_b)]};$$

2. high total ligand limit: $\phi_b \to 1$, $\phi_c \to 0$,

$$Lim\left(\frac{F(t)}{F_0} - 1\right) = \sum_{n=1}^{\infty} \frac{(-\kappa_b)^n}{n![1+n(1+2t/\tau_b)]}.$$

Thus as in other cases the 'high' total ligand limit is just the correct free ligand diffusional recovery with time constant τ_b. However, for the low total ligand case, where most if not all of the ligand will be in the complexed state at any given time (and hence non-fluorescent and non-bleachable) we get the standard diffusional recovery function multiplied by the exponential decay function involving the overall rate of chemical relaxation/reaction R. Note that the R definition in this work is not only a function of the forward and backward rate constants, but also one of the equilibrium concentration of free binding sites. Thus during a total labelled ligand titration series, the actual numerical value of R varies from a minimum of k_b at high c_t to much higher values dominated by $k_f c^a{}_{eq}$ at low c_t.

The key question is whether the recoveries will be faster or slower as a result. Recall, however, that the

PHILOSOPHICAL TRANSACTIONS OF THE ROYAL SOCIETY B BIOLOGICAL SCIENCES

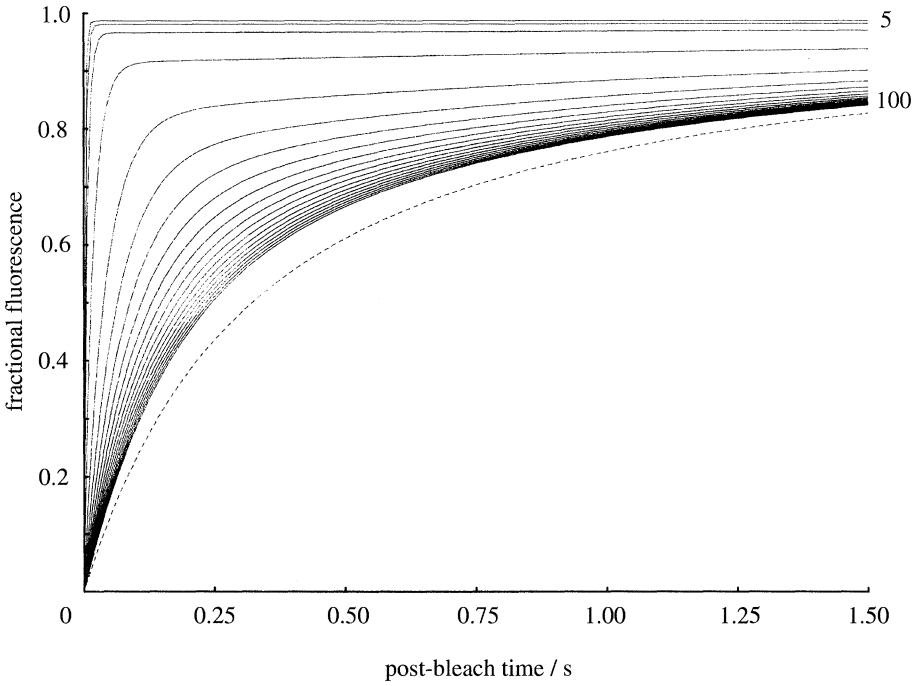

Figure 2. Simulated fractional FRAP curves for the reversible binding model as a function of total labelled ligand (5–100 μM range). The transient complex is assumed to be immobile and completely unbleachable and non-fluorescent. The free diffusant has a bleach constant of 3, a quantum yield of 1 and a diffusion coefficient of 10^{-6} cm^2 s^{-1}. The laser e^{-2} radius is 10 μm. The concentration of binding sites is 20 μM, the forward rate constant k_f is taken as 25 μM^{-1} s^{-1} and the backward rate constant k_b is 5 s^{-1}. The dotted line denotes the pure diffusion recovery curve.

critical central assumption of the entire derivation is that the chemical kinetic rate is considerably bigger (faster) than the diffusional rate, essentially τ_b^{-1}. This means that the exponential multiplier must be a fast-decaying function of time relative to the diffusional series term. Thus for any post-bleach time t, the right hand side of the low total ligand limit (1) must be smaller than the corresponding quantity of (2). Thus the recovery curves approach 1.0 quicker in (1) compared to (2). The FRAP traces will therefore appear to be faster than that expected for pure diffusional exchange of the free ligand. Thus there are some circumstances in which the FRAP method reports primarily on the chemical kinetic rates of binding/unbinding rather than the diffusional rates of the reaction partners. Provided there are sufficient bleaching and quantum yield differences between the free and complexed ligand states, it is possible that the empirical FRAP kinetics will be dominated by chemical interaction rates rather than by diffusional exchange. This will especially be so at 'low' total ligand concentrations, again 'low' being relative to total binding site concentration and the value of K_{eq}^{-1} especially. Figure 2 shows a typical simulation set for this case, with all the curves appearing faster than that due to diffusional exchange alone. The rate of speed-up depends solely on the value of R chosen, and experimentally this may well be unknown. Remember that the objective lateral diffusion coefficient D_b, the e^{-2} beam radius ω, and hence the diffusion time τ_b are constant for all these traces.

Figures 3*a* and *b* take a last simulation case less extreme than the above to demonstrate that the retardation and speeding-up effects can both be evident during a total ligand titration experiment. With all the series terms now involved, it is possible to see the whole range of phenomena as c_t is varied. At very low free fractions for the case simulated, the FRAP curves will look distinctly multi-component with a fast initial rise followed by a much slower major component. If we take the time to reach 50% of the final recovery level as a crude yardstick or single parameter for such curves, we will get apparent diffusion times in the very slow regime. As c_t rises however, the speed-up term highlighted above can become dominant, and apparent diffusional recovery times faster than the true diffusional time for the ligand can occur. As c_t rises further leading to significant ϕ_b, the curves slow again and approach the true value in the limit of large c_t. We emphasise again that this is what the FRAP kinetics will look like to the experimenter, the free-labelled ligand is always diffusing at the same rate for all these curves (complex again assumed immobile in this case). Thus if the experimenter is unaware of the true situation and fits a pure diffusional recovery FRAP function to such data, it will appear that the apparent diffusion coefficients are initially small, then increase to values larger than that obtained with pure ligand alone, and then gradually decrease until the 'correct' values are reached. The greater the value for R and the larger the fluorescence parameter differences are, the greater the potential for anomalous diffusion coefficients to be reported. Figure 3*b* plots the overall halftimes against c_t for the data curves in 3*a*. We emphasise again that the recovery curves in this instance are in reality multi-component, and crude single parameter estimates such

PHILOSOPHICAL TRANSACTIONS OF THE ROYAL SOCIETY B BIOLOGICAL SCIENCES

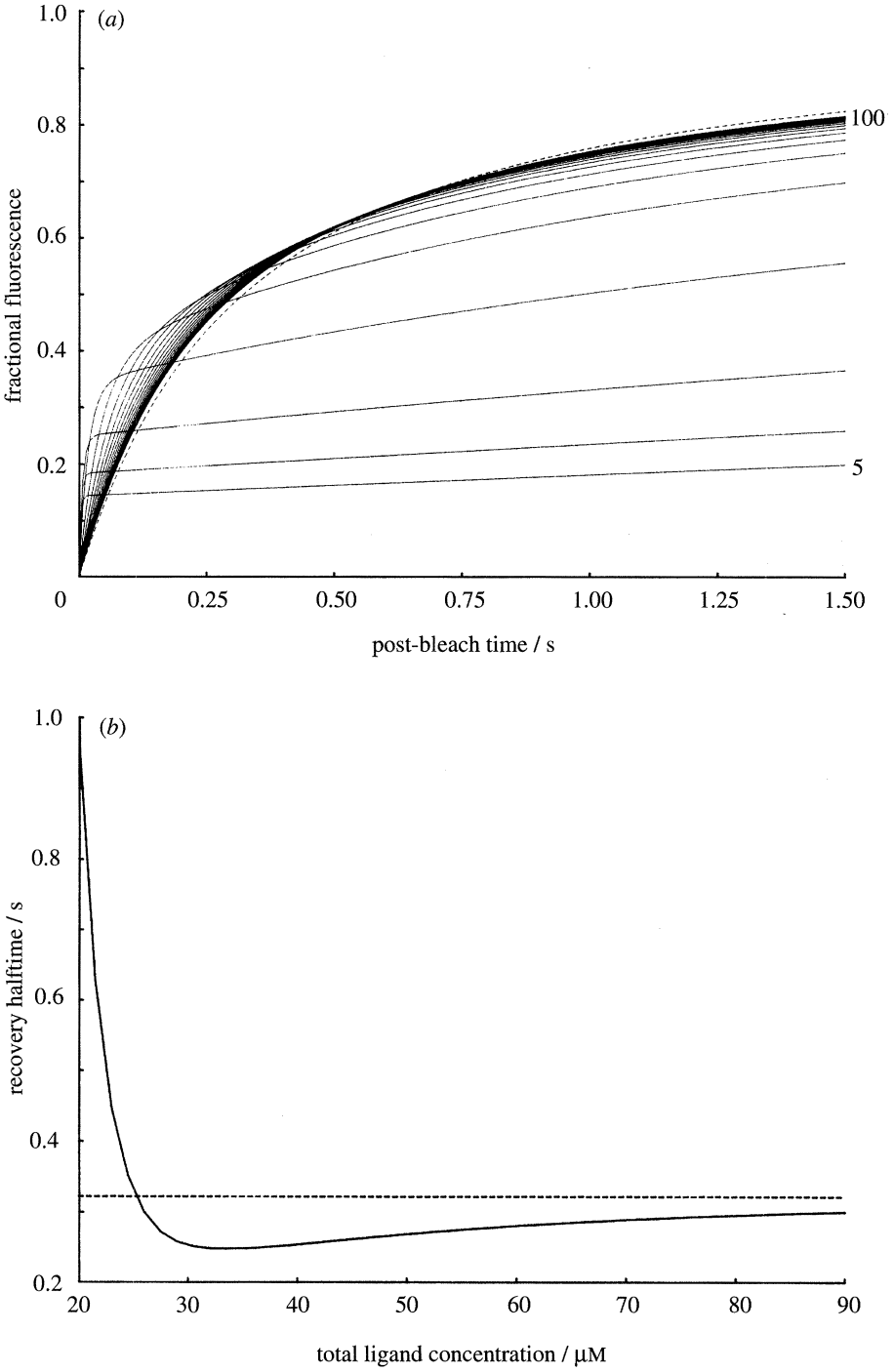

Figure 3. (*a*) Simulated fractional FRAP curves as a function of total labelled ligand (5–100 μM) for a general case where the transient complex is not fully bleach-protected and non-fluorescent. Simulation parameters as in figure 2 with the bleach constant and quantum yield for the bound state taken as 1 and 0.05 respectively. The dotted line again denotes the pure diffusion recovery curve. (*b*) The simulation data of figure 3*a* replotted as 50% recovery halftime (s) as a function of total labelled ligand concentration (μM). The dotted line denotes the pure diffusion result for the free ligand.

as halftimes are not quantitatively adequate. Nevertheless figure 3*b* shows that quite unexpected concentration dependencies can easily arise in FRAP work. If such data sets are correctly modelled and fitted, then FRAP will not only give accurate D_b's, but useful estimates for the chemical interaction rates as well. Significant fluorescence parameter changes upon interaction are necessary for any FRAP sensitivity to these kinetic factors.

(ii) *Reversible binding FRAP effects: numerical simulation approach*

A further insight into the reversible binding phenomenon may be obtained by numerical simulation of the diffusion process. The model adopted here uses a variant of the continuum random walk (CRW) approach (Torquato & Kim 1989) to generate a set of non-interacting trajectories through the pore space of an arbitrary microstructure. These trajectories simu-

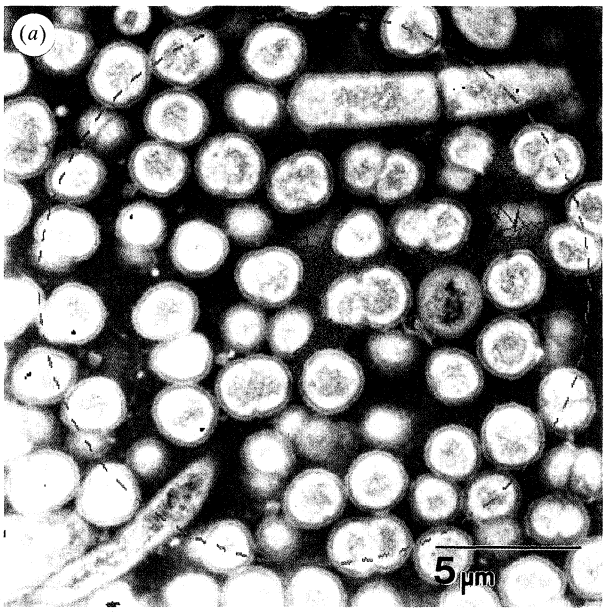

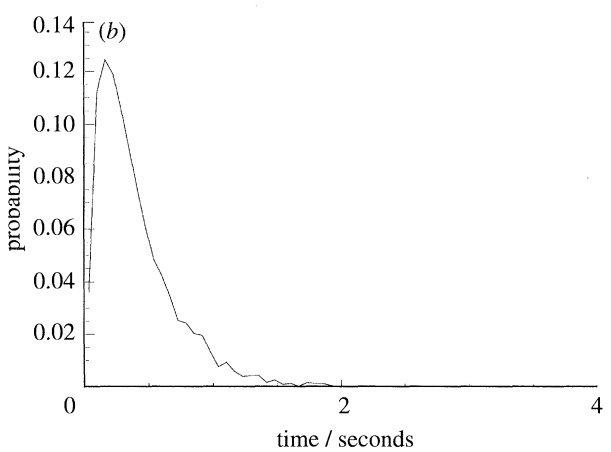

Figure 4. (*a*) Simulated random walk, with optimised step size, through a typical transmission electron microscopy image of a bacterial biofilm. Walk is shown in red and boundary of monitored area, L, is shown in green. (*b*) The distribution of passage times obtained from trajectories through the above microstructure (3000 walks, $D_0 = 10^{-6}$ cm^2 s^{-1}).

late the 'random walk' of the diffusing species but with the step-size optimized for computational efficiency. The real time taken for each step of the trajectory can be calculated if the diffusion coefficient in the pore space (assumed to approximate to that in dilute free solution) is known. The microstructures used in this study were generated from transmission electron micrographs of actual biofilms. Image processing methods were used to enhance the edges of the bacteria within the biofilm and these edges were then fitted with small line segments to form the model structure.

In the example considered in this study each trajectory was started at the centre of a circular region of radius L and then evolved until a point on the region's boundary was reached, whereupon the total real time (the first passage time t_p) for that trajectory was recorded and the process repeated. The geometry ensures that each trajectory is associated with a fixed

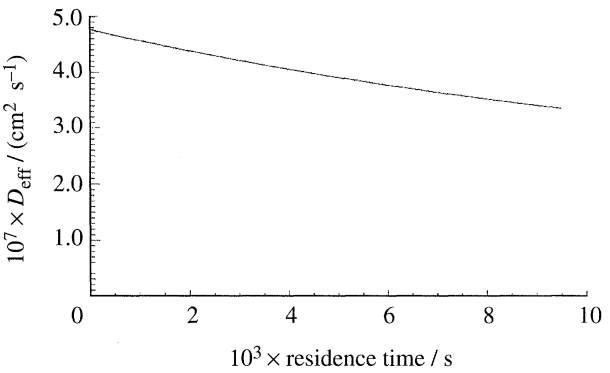

Figure 5. D_{eff} as a function of residence time for the microstructure described in figure 4*a* (3000 walks, $D_0 = 10^{-6}$ cm^2 s^{-1}, active sites 6% of edge segments).

mean square displacement $<$L.L$>$ and as each trajectory is absorbed at the boundary, that multiple beam boundary crossing is avoided. The central quantity generated by this sort of simulation is the distribution ($\rho(t)$) of the first passage times, defined such that $\rho(t)\mathrm{d}t$ is the probability that a randomly chosen trajectory will have a first passage time in the range t to $t+\mathrm{d}t$. To calculate a diffusion coefficient from this distribution we must first evaluate the mean passage time (T_p):

$$T_p = \int_0^\infty t\rho(t)\,\mathrm{d}t,$$

or in terms of the individual trajectories:

$$T_p = 1/\mathrm{N}\sum_i t_i.$$

Because $<$L.L$>$ is fixed, an effective diffusion coefficent (D_{eff}) can then be calculated using the equation:

$$D_{eff} = L^2/4T_p.$$

Typically several thousand trajectories will be needed for an accurate description of ρ(t), whereas as few as two hundred may be sufficient to give a reasonable approximation to T_p and hence D_{eff}.

A walk is illustrated superimposed on figure 4*a*. The $\rho(t)$ of this system constructed using 3000 trajectories is shown in figure 4*b*. Using the T_p value we evaluate the D_{eff}:

$$D_{eff}/D_0 \simeq 0.51.$$

The effect of reversible binding can be modeled by assigning a fraction of the segments used to define the edges in our model as active sites. When a walker is deemed to have 'hit' this point on the surface, it is held there for an appropriate dwell time and then released to continue its walk to the absorbing boundary. The above simulation is repeated with this additional feature and the results are illustrated in figure 5 where we plot D_{eff} as a function of a fixed residence time. For this example we assumed 6% of the edge segments contained active sites randomly distributed over the entire microstructure and that on reaching these sites the particle is certain to bind without any change in quantum efficiency.

PHILOSOPHICAL TRANSACTIONS OF THE ROYAL SOCIETY B BIOLOGICAL SCIENCES

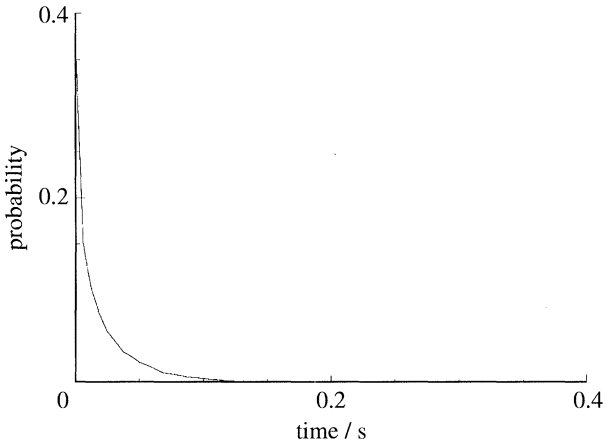

Figure 6. Passage time distribution for reversible binding to active sites, plus fluorescence quenchinmg on binding (3000 walks, $D_0 = 10^{-6}$ cm^2 s^{-1}, active sites 6% of edge segments, 30% probability of no fluorescence on binding).

The third example is designed to show the effect of fluorescence quenching on binding. We use the same environment as above with the same active site distribution, but this time introduce the factor that on binding there is a 30% probability that the particle will stop fluorescing until released. When this is programmed to happen we end the walk at that point and start a new one when the particle is released from binding. The distribution of 'passage times' for these chopped walks is illustrated in figure 6. On comparing the two distributions (figure 4*b* and figure 6) two features can be seen.

1. The distribution is skewed to much smaller times with a corresponding reduction in the apparent mean passage time.

2. The shape of the distribution bears no relation to a gaussian, a pointer to the fact that an interpretation in terms of a simple diffusion process is not sufficient.

If we proceed in the spirit of the basic macroscopic model to attempt to calculate an effective diffusion coefficient by assuming, as that model would, that every walk fragment represented a real walk starting at the centre and leaving at the absorbing boundary, we find a value of:

$$D_{\mathrm{eff}}/D_0 = 9.83,$$

which is clearly unphysical in terms of pure motional phenomena.

If this situation were taken to the extreme with a very large number of binding sites each with a high probability of fluorescence quenching we would lose the ability to say anything about the diffusional

Table 2. *Biofilm diffusion results*

(Figures in brackets are standard deviations.)

description	number of analyses	mean beam diameter / μm	mean $D_{\mathrm{eff}} \times 10^6$ / cm^2 s^{-1}	range of $D_{\mathrm{eff}} \times 10^6$ / cm^2 s^{-1}
solution controls				
kDa dextran				
10	50	9.692 (0.262)	1.761 (0.242)	1.432 → 2.030
40	30	9.373 (0.110)	0.812 (0.079)	0.723 → 0.874
500	10	10.210 (0.06)	0.451 (0.008)	N/A
sucrose starved biofilms				
kDa dextran				
10	7	8.009 (0.317)	0.438 (0.086)	0.320 → 0.522
40	6	9.120 (0.590)	0.494 (0.107)	0.386 → 0.639
500	4	10.755 (0.536)	0.293 (0.055)	0.214 → 0.338
sucrose supplemented biofilms kDa dextran				
10	6	16.548 (0.286)	1.567 (0.238)	1.225 → 1.916
40	6	17.977 (2.397)	1.051 (0.278)	0.563 → 1.390
500	6	13.185 (4.248)	0.219 (0.096)	0.125 → 0.384
ex vivo plaque				
10 kDa dextran				
dense region	6	13.397 (2.256)	2.569 (0.671)	1.837 → 3.617
sparse region	3	11.313 (0.696)	1.962 (0.194)	1.776 → 2.163

PHILOSOPHICAL TRANSACTIONS OF THE ROYAL SOCIETY B BIOLOGICAL SCIENCES

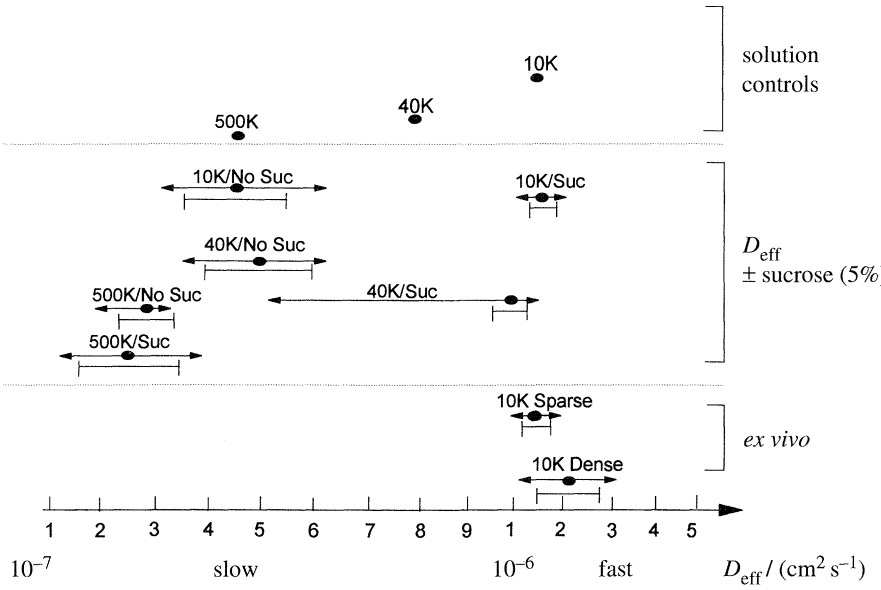

Figure 7. Summary of measured apparent diffusion coefficients for dextrans in free solution, sucrose starved and sucrose supplemented biofilms and *ex vivo* plaque. Mean diffusion coefficients are marked with a solid dot, arrows denote the full spread of data around the mean and closed lines denote the standard deviation about the mean.

processes at all. The whole recovery curve becomes dominated by the effect of the binding process. In such cases the average passage time calculated from the chopped walks distribution becomes a measure of the mean time between binding events (or its inverse the frequency of binding).

(*c*) *Concluding remarks*

The apparently simple kinetic scheme of A reacting reversibly with B to produce transient complex C can yield surprisingly complex FRAP situations. The experimenter may be quite unaware (as we were initially) that some reversible interaction is occurring between the tagged diffusant and the matrix through which it is diffusing. The fact that the recoveries are empirically complete says nothing about the situation, other than ruling out a permanent complex. Standard data analysis could then give quite strange results, with the apparent diffusion coefficients possibly reporting on chemical exchange rates not diffusional exchange. The planktonic dataset (§3*a*) with the strong bleach protection (as the total probe concentration was reduced) and the curious faster-than-maximum probe diffusion result, can now be rationalized using both analytic and numerical methods. The only additional assumption we have to make to get the fourfold speed-up is that there is a strong quantum yield reduction for the FITC-tag when the dextran is complexed with the bacterial surface. The empirical fact of strong bleach protection would support substantial microenvironmental changes around the label sites, which would then be expected to show some quantum yield alterations. Because of the complexity of the general case, no attempt to globally fit the set of traces for the planktonic case has yet been made. We are however confident that the general features of the reversible binding model do in fact hold, and that in particular the recovery rates for the high density case principally reflect the rate of chemical relaxation rather than the rate of pure diffusional exchange.

4. DIFFUSIONAL MEASUREMENTS ON BACTERIAL BIOFILMS

The diffusional characteristics of FITC-conjugated dextrans within *in vitro* bacterial biofilms and *ex vivo* oral plaques have been investigated using FRAP. In particular the effect of providing sucrose nutrient has been examined, which indirectly affects the bacterial ecology, the packing density of the bacteria, the extracellular polymers produced and the composition of the plaque fluid. The influence of reversible probe binding on the measured diffusion rates has been considered at some length for planktonic bacterial suspensions. These effects will also be important for biofilms, however now the measurements are further complicated by local microstructural variations. This makes quantitative interpretation of the data even more difficult, but extension of the numerical methods outlined for planktonic suspensions, allied with images of the gross biofilm structures, may at least provide a framework for our understanding.

(*a*) *Results*

The diffusion rates of a range of dextran probes (10 kDa, 40 kDa and 500 kDa) measured in free solution and within mixed consortium biofilms are summarized in table 2 and are presented graphically in figure 7. All recoveries were complete and very good fits with standard 2-D $f(t)$ were obtained in all cases. Typical bleach depths were 60 %. In table 2, the number of individual analyses, the mean e^{-2} beam radius and the mean and range of the effective diffusion coefficients (D_{eff}) are quoted. Because biofilm microstructure is extremely heterogenous and each set of FRAP traces only covers a relatively small area (ca. 10 μm), it is important to include the whole variation

PHILOSOPHICAL TRANSACTIONS OF THE ROYAL SOCIETY B BIOLOGICAL SCIENCES

in measured values, by quoting the spread of D_{eff}. It is also useful to consider the mean D_{eff}s for each dextran by combining the values measured from distinct biofilm areas. The bulk of measured values may be similar, whilst extreme outliers arise. In these cases the standard deviation of D_{eff} gives an indication of significant differences in diffusion rate over the 'average' biofilm.

The diffusion rates measured for dextran in bacteria free solution (D_{aq}) follow the expected trend, scaling inversely with molecular mass from 10^{-6} cm^2 s^{-1} for the 10 kDa dextran to 10^{-7} cm^2 s^{-1} for the 500 kDa dextran. These measured values compare well with calculated diffusion coefficients (Lawrence *et al.* 1994) based upon molecular hydrodynamic radius and radius of gyration.

The sucrose starved biofilm experiments showed a significant decrease in measured diffusion coefficients compared to D_{aq} for all sizes of dextran probe. This effect was most marked for the 10 kDa probe (fourfold decrease). The spread and standard deviations of the diffusion rates were small for all molecular masses of dextran. This indicates that the microstructure of these biofilms is reasonably homogeneous, an observation which is supported by DIC optical microscopy of these specimens (see figure 8*a*). These biofilms are of uniform thickness and density and comprise large areas of tightly packed streptococcal bacteria.

The sucrose supplemented biofilms were quite different. The mean effective laser beam radius increased dramatically (see figure 9), most noticeably in regions of dense bacterial packing. However some of these regions were no more densely packed than areas within the sucrose starved biofilms, suggesting that extracellular material was increasing scattering. For the 10 kDa probe the D_{eff} was virtually identical to D_{aq} and both the spread and standard deviation of values was small. The mean D_{eff} values for the 40 kDa probe showed an increase in apparent diffusion rate over the bacteria-free control. This difference is statistically significant and represents a speeding up of the probe within the biofilm of ca. 30%. The spread of values in this case was high and the slowest D_{eff}s measured overlap with the faster 40 kDa probes measured in sucrose starved biofilms. For the 500 kDa probe, D_{eff} is slower than D_{aq} and the diffusion rate falls in line with that observed in the sucrose starved biofilm.

Microscopy of sucrose supplemented biofilms supports the idea that these are microstructurally heterogeneous (see figures 8*b*, 10*a*, *b*). The density of biofilm coverage and the film thickness vary markedly across the specimen (from monolayers of bacteria to ca. 200 μm thick films). The structure is clearly more open than in the sucrose starved case and much more extracelluar polymer is observed.

Ex vivo, intact oral plaques were obtained fresh from human subjects. In this case the biofilm structure was so clearly heterogenous that the measured diffusion rates were divided into two groups for each dextran, termed sparse and dense. Again, DIC optical micrographs confirm this gross heterogeneity (see figure 8*c*). The 10 kDa dextran probe in sparse regions of plaque gave apparent diffusion rates identical to those measured in free solution. In dense regions of plaque the mean apparent diffusion rates were faster than free solution values, although in this instance the difference was not significant.

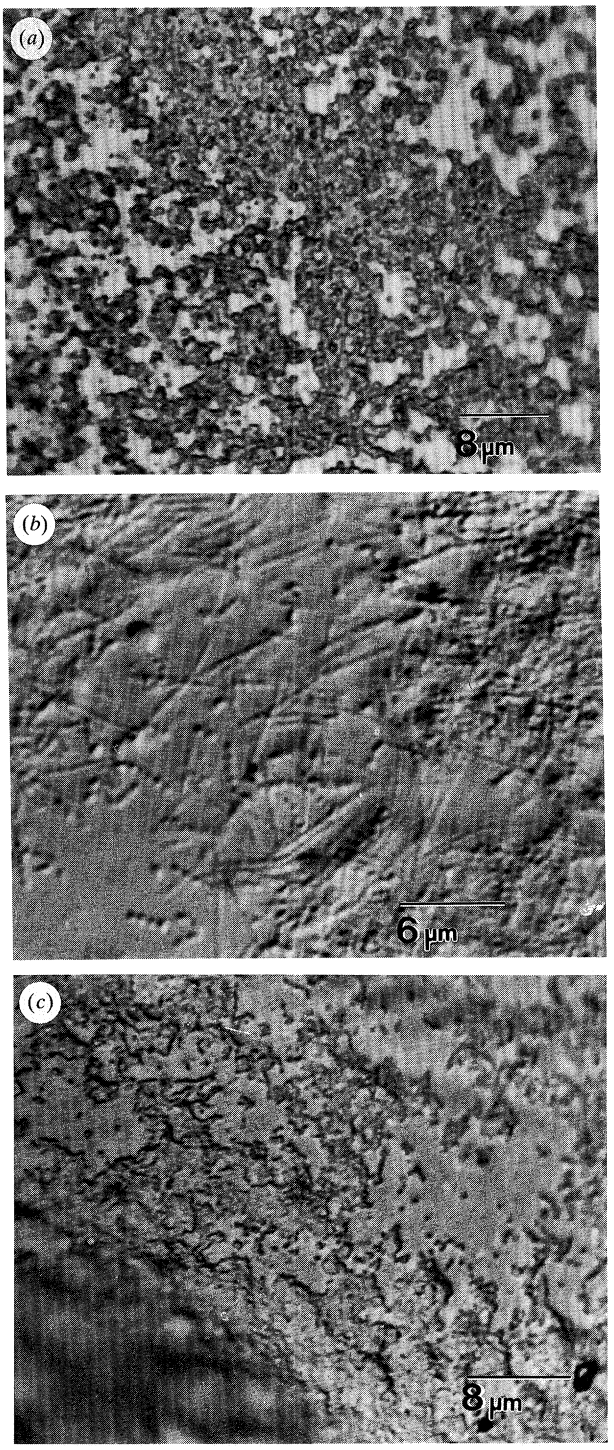

Figure 8. Differential interference contrast optical micrographs of bacterial biofilms: (*a*) sucrose starved *in vitro* biofilm; (*b*) sucrose supplemented *in vitro* biofilm; and (*c*) *ex vivo* plaque.

(*b*) *Discussion*

In this study the measured effective diffusion coefficients divide quite clearly between those measured in sucrose starved and sucrose supplemented biofilms (see figure 7). In the former case the diffusion rates are severely attenuated when compared to free

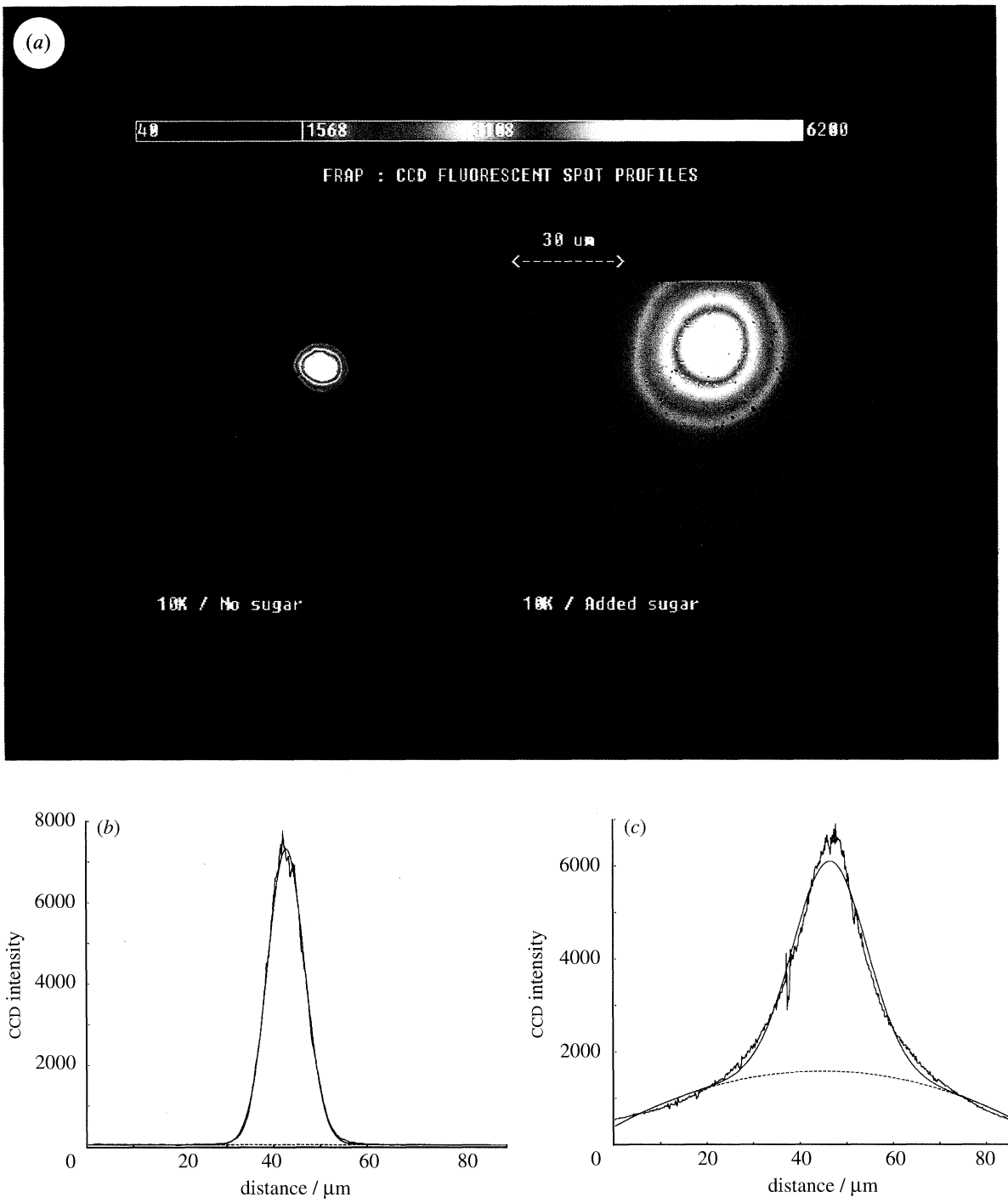

Figure 9. CCD Fluorescent spot images taken under non-bleaching conditions for 10 kDa dextran in either sucrose-starved (top-left) or sucrose supplemented (top-right) *in vitro* biofilms. Central horizontal sections through these images are shown in the bottom-left (non-sucrose) and bottom-right (sucrose supplemented) panels, along with nonlinear least-squares curvefits of the data to a gaussian profile and a quadratic background polynomial (dotted line).

solution values over all molecular masses of dextran probe. The spread and standard deviation of these diffusion rates are small, indicating that sucrose starved biofilms are microstructurally quite uniform, a fact which has been confirmed by optical microscopy. The change in diffusion rate over free solution is most marked at low molecular mass, which might imply that the smaller probes are capable of greater penetration of the biofilm. Overall, it appears that the tortuous paths through the biofilm microstructure are having a significant effect on the measured diffusion rate. These biofilms do not contain high levels of extracellular polymer, so it may be inferred that the number of transient binding sites is low when compared to the high levels of free probe.

The situation is quite different for sucrose supplemented biofilms which have undergone changes in bacterial ecology, microstructure and extracellular polymer production. Provision of sucrose dramatically increases the relative numbers of *S. mutans* and *L. casei* (Bradshaw *et al.* 1992). The sucrose also greatly increases extracelluar glucan production, leading to a

PHILOSOPHICAL TRANSACTIONS OF THE ROYAL SOCIETY B BIOLOGICAL SCIENCES

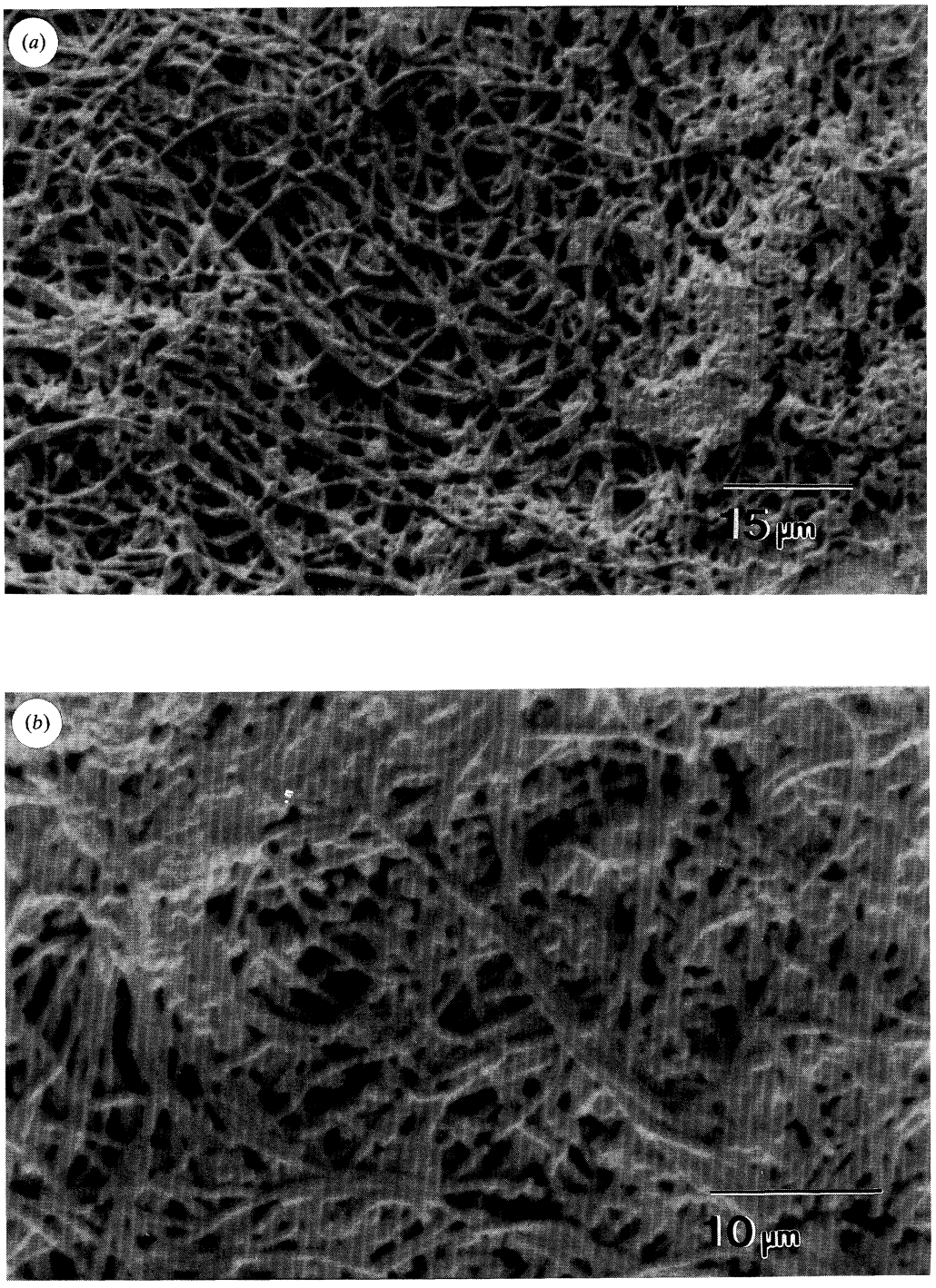

Figure 10. Low temperature scanning electron micrographs of sucrose supplemented *in vitro* biofilms: (*a*) low magnification, showing an open bacterial network; and (*b*) high magnification, showing the variety of bacterial morphologies and extracellular material.

much more open bacterial network. These changes transform biofilm microstructure and consequently binding site availability, both of which will directly affect apparent probe diffusion. This is borne out by the observed diffusion rates. The opening of the biofilm structure would be expected to produce an increase in diffusion rate, however this alone cannot account for some of the extreme increases observed. In particular biofilm regions, the 40 kDa probe was diffusing faster than in free solution, implying that some reversible binding was occurring. Increasing the relative amount of extracellular polymer within the biofilm produces two effects; additional specific reversible binding sites and increased non-specific reversible binding due to extra available surface area. This is in effect the same as decreasing the concentration of free probe in the titration carried out in §3.

In intact human plaques there was extreme microstructural heterogeneity across the substrate. The mean apparent diffusion rates for sparse regions were identical to free solution values for a 10 kDa dextran probe. In these areas the bacteria were so well dispersed that the bulk of the FRAP recovery was due to simple diffusion in free solution. In dense areas the diffusion

rate was marginally faster than free solution but there was a large spread of values, some of which were significantly faster than free solution. This would indicate that reversible binding is an important factor in controlling apparent diffusion rate in these plaque samples. Overall, the intact human plaques appear to match the sucrose treated *in vitro* biofilms most closely (which is not surprising as they were sucrose supplemented), showing the marked influence of extracellular polymer on probe binding.

It is not possible from our current position to deconvolute the influences of tortuosity and reversible binding on apparent probe diffusion rate and indeed the spread of values obtained within a single biofilm would indicate that there are large local variations in these factors. Numerical and analytical modelling have allowed us to gauge how these factors will influence effective diffusion rates and this broadly correlates with our observations.

It is important that we consider the likely nature of the reversible binding sites within our biofilms, as this may help in designing future experiments to probe the reversible binding phenomenon. Several groups have identified glucan (dextran) binding moieties within oral plaques, which are thought to mediate interactions important in bacterial adherence (Clark & Gibbons 1977; Staat *et al.* 1980). The initial observations were based on the agglutination of bacteria by high molecular mass dextrans. *S. sobrinus* strains aggregate rapidly in the presence of dextran, whereas weaker interactions are seen for *S. mutans*. From these observations it was suggested that specific glucan binding adhesins may exist on the cell surface. Several of these adhesins have now been isolated and characterized. Both *S. sobrinus* and *S. mutans* produce multiple glucosyltransferase (GTF) isoenzymes which display a high affinity for glucan (Mooser & Wong 1988). In addition a family of non-enzymatic glucan binding proteins (GBP) have been isolated. For example, Landale & McCabe (1987) isolated a 15 kDa GBP from *S. sobrinus* 6715–49, Russell (1979) isolated a 74 kDa GBP from *S. mutans* 3209 and Wu-Yuan & Gill (1992) isolated a 87 kDa GBP from *S. sobrinus* B13. These proteins are all cell surface bound, making accessibility a major issue in a complex biofilm. Also, the expression of these moieties is now known to depend on the bacterial microenvironment (Brown & Williams 1985), making predictions about the number of binding sites extremely difficult. A further complication is the potential for non-specific reversible binding, between the bulk extracelluar matrix and the probe. The nature of such interactions are merely conjecture. What is clear is that an increase of sucrose nutrient will lead to higher relative levels of *S. sobrinus* and *S. mutans* in the biofilm. This leads to a direct increase in the number of specific glucan binding sites. Concomitant with this an increase in the level of extracelluar polymer produces a larger surface area of material, capable of non-specific interaction.

Previous studies of molecular diffusion rates through biofilms, using indirect methods, have measured decreases of two to fivefold over the values for free solution (Charcklis & Marshall 1990). These figures fall in line with the extent of slowing which we observed in non-supplemented biofilms for dextran probes, particularly if we consider that the molecules and ions studied previously were small (for example, ammonia, nitrate, bromide, sodium). However, two studies are worth particular comment: work by Tatevossian (1985) on sucrose diffusion in human dental plaque and work by Lawrence *et al.* (1994) on dextran diffusion in *Pseudomonas* biofilms. In both cases the reported diffusion rates within the biofilms are significantly slower (20- to 50-fold) than those reported here.

The work of Tatevossian used ^{14}C radiolabelled sucrose as a probe in reconstituted, centrifuged human plaque. He observed that increasing the plaque tortuosity, by increasing the centrifugal packing force reduced the diffusion rate significantly. In essence, this work focuses solely on the influence of tortuosity on diffusion. The fact that plaques are pooled and centrifuged before examination will destroy any microstructural features which might allow preferential diffusion. Thus any diffusion rate measurement is likely to be significantly lower than within an intact biofilm. Tatevossian also examined the effect of extracellular material on diffusion rate and made the slightly confusing observation that experimental conditions which increased the extracellular glucan in human plaque produced a reduction in the apparent rate of sucrose diffusion, whereas similar conditions in centrifuged batch cultures of *S. mutans* increased the diffusion rate. He suggests that certain unique extracellular protein components may be present in human plaque, which lead to slower diffusion with increasing extracellular polymer. We have no evidence for such an effect in our systems and it may be that the observed differences again arise from the packing methods used.

Lawrence *et al.* (1994) recently published work using confocal imaging to assess diffusion of fluorescently tagged dextrans within biofilms. This is clearly very close to the scenarios examined in this study, the only major experimental difference being that all their tabulated diffusion data refers to confocal imaging of probe influx to/ efflux from a biofilm rather than FRAP. They reported an apparent slow-down factor relative to free solution for a 40 kDa dextran of about 40-fold, which compares to our maximum of about threefold. This is obviously quite troubling and prompted us to examine their data analysis procedure in more detail. Because the precise details of their biofilms and data analysis methods are sketchy, we have derived a plausible generalized analytical solution as follows.

Assuming a pure 1-D-diffusional recovery mechanism, we obtain the following Fourier series solution for the fluorophore concentration as a function of time (after external medium switch) and distance in an initially uniformly loaded biofilm:

$$c(x,\,t) = \frac{4C_0}{\pi} \sum_{n=0}^{\infty} \frac{(-1)^{n+1}}{(2n+1)} \times \exp(-(2n+1)^2\,\pi^2 Dt/4h^2) \cos\left(\frac{(2n+1)\pi(x+h)}{2h}\right).$$

This is the solution valid over $-h < x < 0$, where h is the

PHILOSOPHICAL TRANSACTIONS OF THE ROYAL SOCIETY B BIOLOGICAL SCIENCES

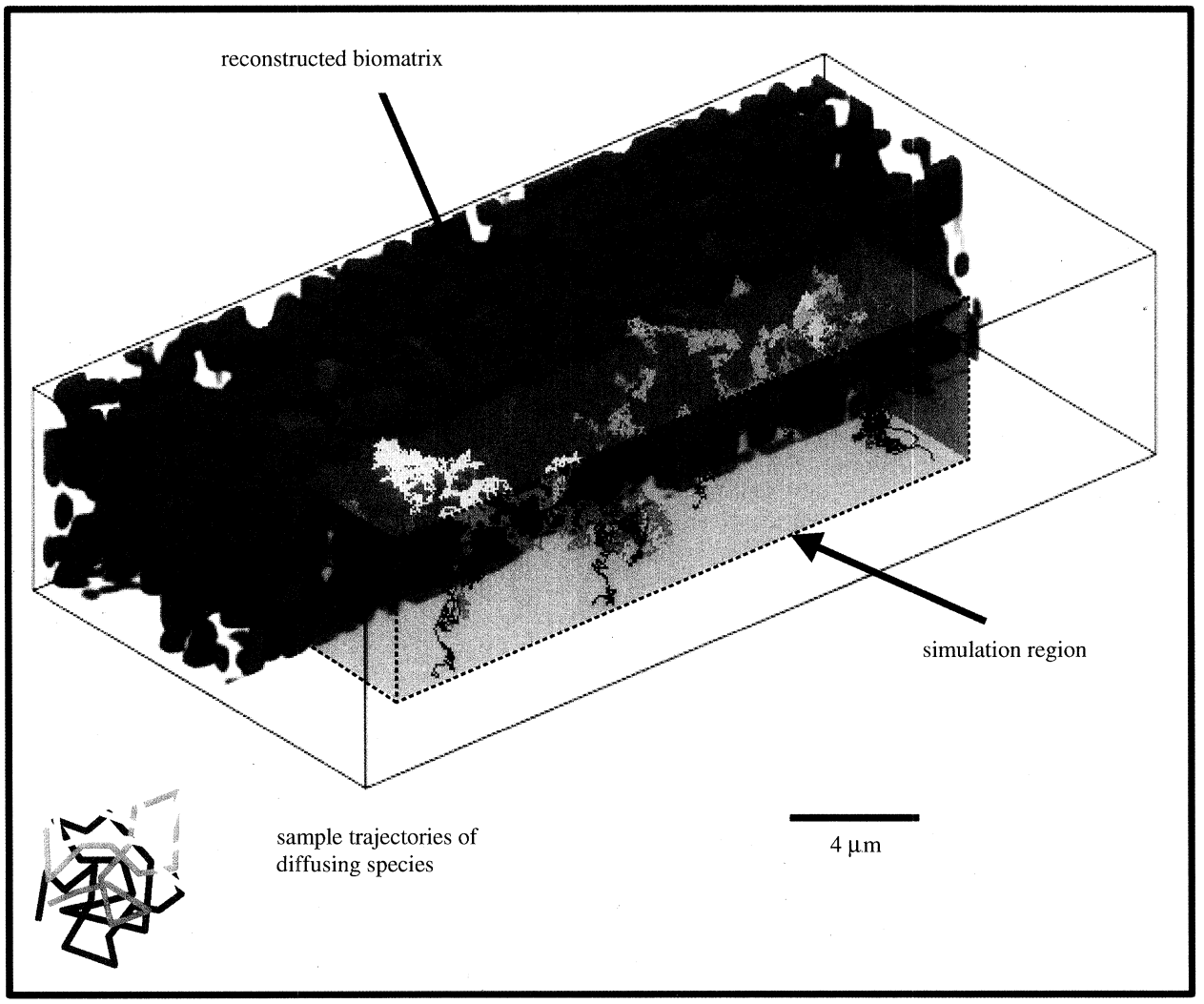

Figure 11. Random walks through a 3-D reconstructed biofilm, obtained from a set of confocal laser scanning microscopy images. Rendered biofilm microstructure is shown on the left (green). Walks, begun at the top surface of the biofilm, are shown on right (brown and red).

thickness of the biofilm and D, the one-dimensional diffusion coefficient, with c_0 denoting the initial $t = 0$ uniform loading condition. The boundary conditions assumed were that of zero flux at the biofilm base (impermeable biofilm support) and zero maintained concentration at the top of the biofilm. This is our interpretation of the verbal description given by Lawrence *et al.* (1994). It is interesting to estimate the 50% efflux times for an assumed biofilm thickness (40 µm) with confocal monitoring some 5 µm off the lower surface, for a range of assumed diffusion coefficients. Both the biofilm thickness and monitoring depth are as given in Lawrence *et al.* (1994). According to this expression, a measured 50% efflux time of about 20 s (40 kDa dextran raw efflux data of Lawrence *et al.* 1994) would equate to a diffusion coefficient of about 3×10^{-7} cm^2 s^{-1} rather than the value tabulated by Lawrence *et al.* (1994) of 1.7×10^{-8} cm^2 s^{-1}. Thus the raw efflux data translate to considerably faster diffusion coefficients using the analysis described here, compared to the analysis methods originally employed. If our re-analysis is correct, the biofilm slow-down factors relative to free solution then become similar to those of this paper i.e. two-threefold rather than 40-fold.

The FRAP technique as used in this study is a convenient and fast method for determining the apparent diffusional behaviour of tagged macromolecules in biofilm environments. It is obvious however that the current method implemented here lacks a critical imaging capability of the matrix microstructure i.e. the diffusional measurements cannot be put into a precise spatial context. Such a microstructure map could form the basis for numerical diffusional modelling as described in §3*b* leading to a predicted diffusional image. This could then be compared to the experimental diffusional image and the supposed processes (local binding with or without fluorescence changes etc.) altered until a best-fit of the images were obtained. This principle has been tested recently by performing 3-D diffusion simulations through a rendered biofilm image obtained using confocal microscopy (see figure 11).

While this work continues, the problem remains of obtaining diffusion maps. A confocal-FRAP implementation reported elsewhere offers diffusional measurements at precise spatial locations in 3-D, but so that sufficient instrumental speed be available, one of the spatial imaging axes has had to be sacrificed (Blonk *et*

al. 1993). Thus the FRAP image in this method comprises one spatial axis through the bleached spot, with the other axis being recovery time. Alternative strategies have also been described in the literature maintaining two spatial imaging axes but with consequent severe limitations on the sample recovery times (Peters & Scholz 1990; Sauer *et al.* 1991). Non-FRAP possibilities also exist using highly fluorescent tracker particles to directly follow the diffusion paths (Anderson *et al.* 1992).

The necessity for parallel imaging and diffusional measurements is substantially increased if reversible binding phenomena are occurring. The detection of binding from diffusional measurements such as FRAP is at best indirect, except in the case of irreversible binding. We have seen that quantitative allowance can in principle be made for the reversible binding phenomena, but this could be expensive as regards experimental and analysis times. It might be better to address the binding issue more directly, by imaging non-diffusional phenomena. One exciting possibility would be to complement fluorescence resonance energy transfer (FRET) imaging with a fast confocal-FRAP variant. FRET depends on very close molecular proximity between two fluorophores, labelled donor and acceptor. Imaging of acceptor fluorescence when excitation wavelengths tuned for the donor are used, would result in a proximity or interaction map for the chromophore pair. In the biofilm case, suppose all the bacterial membranes were labelled with a donor fluidity label and that the external macromolecule carried a suitable acceptor tag. Then the appearance of FRET signals would flag specific interaction sites. It may be also possible to exploit whatever intrinsic fluorescence signals the bacteria already possess (tryptophan, tyrosine) so as to act as the donor fluorophore. Such qualitative FRET-images could be put on a quantitative footing by using fluorescence lifetime imaging (FLIM) of the donor emission lifetime. It is also known that the photobleaching efficiency of the donor alters upon energy transfer (Jovin *et al.* 1989; Gadella *et al.* 1993). Thus FLIM, FRET and a fast 2-D imaging FRAP variant yet to be devised may offer a versatile experimental route to image both the apparent diffusional rates and the interaction phenomena.

We thank Dr P. D. Marsh and Dr D. J. Bradshaw (PHLS-CAMR, Salisbury, U.K.) for providing *in vitro* biofilms, Dr S. Singleton and Dr C. Allison for providing confocal images of biofilms, Dr J. Ashdown for useful discussion and Mrs J. E. Munro-Brown, Ms A. Griffiths, Mr M. P. Ashton and Mr O. Gallagher for technical assistance with routine microbiology and microscopy.

REFERENCES

Anderson, C. M., Georgiou, G. N., Morrison, I. E. G., Stevenson, G. V. W. & Cherry, R. J. 1992 Tracking of cell surface receptors by fluorescence digital imaging microscopy using a charge-coupled device camera: low density lipoprotein and influenza virus receptor mobility at 4 °C. *J. Cell. Sci.* **101**, 415–425.

Aragon, S. R. & Pecora, R. 1975 Fluorescence Correlation Spectroscopy and Brownian Rotational Diffusion. *Biopolymers* **14**, 119–138.

Axelrod, D., Koppel, D. E., Schlessinger, J., Elson, E. L. & Webb, W. W. 1976 Mobility measurements by analysis of fluorescence recovery kinetics. *Biophys. J.* **16**, 1055–1069.

Baltimore, R. S. & Mitchell, M. 1980 Immunologic investigations of mucoid strains of *Pseudomonas aeruginosa*. *J. Infect. Dis.* **141**, 238–247.

Bevington, P. R. 1969 *Data reduction and error analysis for the physical sciences*, pp. 204–246. New YorK: McGraw-Hill.

Blonk, J. C. G., Don, A., van Aalst, H. & Birmingham, J. J. 1993 Fluorescence photobleaching recovery in the confocal scanning light microscope. *J. Microsc.* **169**, 363–374.

Bracewell, R. N. 1986 *The Fourier transform and its applications*, edn 2, pp. 244–250. *New York*: *McGraw-Hill.*

Bradshaw, D. J., McKee, A. S. & Marsh, P. D. 1989 Prevention of population shifts in oral microbial communities *in vitro* by low fluoride concentrations. *J. Dent. Res.* **68**, 1298–1302.

Bradshaw, D. J., Marsh, P. D., Watson, G. K. & Cummins, D. 1992 A modified chemostat system to study the ecology of oral biofilms. *J. Dent. Res.* **71**, 674.

Brown, M. R. W. & Williams, P. 1985 The influence of environment on envelope properties affecting survival of bacterial infections. *A. Rev. Microbiol.* **39**, 527–556.

Capdeville, B., Nguyen, K. M. & Rols, J. L. 1993 Biofilm modelling: structural, reactional and diffusional aspects. *NATO ASI Ser.* **223**, 251–276.

Characklis, W. G. & Marshall, K. C. (eds) 1990 *Biofilms.* Toronto: Wiley Interscience.

Clark, W. B. & Gibbons, R. J. 1977 Influence of salivary components and extracellular polysaccharide synthesis from sucrose on attachment of *Streptococcus mutans* 6715 to hydroxyapatite surfaces. *Infect. Immun.* **18**, 514–523.

Costerton, J. W., Cheng, K. J., Geesey, G. G., Ladd, T. I., Nickel, J. C., Dasgupta, M. & Marrie, T. J. 1987 Bacterial biofilms in nature and disease. *A. Rev. Microbiol.* **41**, 435–464.

Costerton, J. W. 1994 Structure of biofilms. In *Biofoul. Biocorr. Ind. Water Syst.* (ed. G. G. Geesey), pp. 1–14. Boca-Raton: Lewis.

Costerton, J. W., Lewandowski, Z., DeBeer, D., Caldwell, D., Korber, D. & James, G. 1994 Biofilms, the customised microniche. *J. Bact.* **176** 2137–2142.

Cummins, D., Moss, M. C., Jones, C. L., Howard, C. V. & Cummins, P. G. 1992 *Bin. Comput. Microbiol.* **4**, 86–92.

Dibdin, G. H. 1981 Diffusion of sugars and carboxylic acids through human dental plaque *in vitro*. *Arch. Oral Biol.* **26**, 515–523.

Dibdin, G. H. 1992 A finite-difference computer model of solute diffusion in bacterial films with simultaneous metabolism and chemical reaction. *Comput. Appl. Biosci.* **8**, 489–500.

Edgar, W. M. (ed.) 1989 Symposium on Plaque Fluid: Biochemistry and Properties of the Plaque/Enamel Interface. *J. Dent. Res.* **69**, 1307–1342.

Ehrenberg, M. & Rigler, R. 1976 Fluorescence correlation spectroscopy applied to rotational diffusion of macromolecules. *Q. Rev. Biophys.* **9**, 69–81.

Elson, E. L. & Magde, D. 1974 Fluorescence Correlation Spectroscopy I. Conceptual basis and theory. *Biopolymers* **13**, 1–27.

Elson, E. L. 1986 Membrane dynamics studied by fluorescence correlation spectroscopy and photobleaching recovery. *Rev. Soc. Gen. Physiol.* **40**, 367–383.

Elson, E. L. 1985 Fluorescence Correlation Spectroscopy and Photobleaching Recovery. *A. Rev. phys. Chem.* **36**, 379–406.

Gadella, T. W. J., Jovin, T. M. & Clegg, R. M. 1993 Fluorescence Lifetime Imaging Microscopy (FLIM):

PHILOSOPHICAL TRANSACTIONS OF THE ROYAL SOCIETY B BIOLOGICAL SCIENCES

spatial resolution of microstructures on the nanosecond time scale. *Biophys. Chem.* **48**, 221–239.

Garland, P. B. 1981 Fluorescence photobleaching recovery: control of laser intensities with an acousto-optic modulator. *Biophys. J.* **33**, 481–482.

Geesey, G. G., Stupy, M. W. & Bremer, P. J. 1992 The dynamics of biofilms. *Int. Biodeter. Biodeg.* **30**, 135–154.

Govan, J. R. W. 1975 Mucoid strains of *Pseudomonas aeruginosa*. *J. med. Microbiol.* **8**, 513–522.

Hurewicz, W. 1975 *Lectures on ordinary differential equations*, pp. 34–43. Cambridge, Massachusetts: M.I.T. Press.

Jovin, T. M., Marriott, G., Clegg, R. M. & Arndt-Jovin, D. J. 1989 Photophysical processes exploited in digital imaging microscopy: fluorescence resonance energy transfer and delayed luminescence. *Ber. BunsenGes. phys. Chem.* **93**, 387–3.

Kolenbrander, P. E. 1991 Coaggregation adherence in human microbial ecosystems. In *Microbial cell–cell interactions* (ed. M. Dworkin), pp. 303–329. Washington: American Society of Microbiology.

Landale, E. C. & McCabe, M. M. 1987 Characterisation by affinity electropheresis of an α-1,6-glucan-binding protein from *Streptococcus sobrinus*. *Infect. Immun.* **55**, 3011–3016.

Lawrence, J. R., Korber, D. R., Hoyle, B. D., Costerton, J. W. & Caldwell, D. E. 1991 Optical sectioning of microbial biofilms. *J. Bact.* **173**, 6558–6567.

Lawrence, J. R., Wolfaardt, G. M. & Korber, D. R. 1994 Determination of diffusion coefficients in biofilms by confocal laser microscopy. *Appl. Envir. Microbiol.* **60**, 1166–1173.

Magde, D., Elson, E. L. & Webb, W. W. 1972 Thermodynamic fluctuations in a reacting system – measurement by fluorescence correlation spectroscopy. *Phys. Rev. Lett.* **29**, 705–708.

Magde, D., Elson, E. L. & Webb, W. W. 1974 Fluorescence correlation spectroscopy II An experimental realization. *Biopolymers* **13**, 29–61.

Marquardt, D. W. 1963 An algorithm for least-squares estimation of nonlinear parameters. *J. Soc. Ind. Appl. Math.* **11**, 431–441.

McNee, S. G., Geddes, D. A. M., Weetman, D. A. & Beeley, J. A. 1982 Diffusion of sugars and acid in human plaque *in vitro*. *Arch. Oral Biol.* **27**, 975–979.

Mets, U. & Rigler, R. 1994 Submillisecond detection of single rhodamine molecules in water. *J. Fluoresc.* **4**, 259–264.

Meyer, T. & Schindler, H. 1988 Particle counting by fluorescence correlation spectroscopy. *Biophys. J.* **54**, 983–993.

Mooser, G. & Wong, C. 1988 Isolation of a glucan binding domain of glucosyltransferase from *Streptococcus sobrinus*. *Infect. Immun.* **56**, 880–884.

Nickel, J. C., Rueska, I., Whitfield, C., Marrie, T. J. & Costerton, J. W. 1985 Tobramycin resistance in *Pseudomonas aeruginosa* cells grown as a biofilm on urinary catheter material. *Eur. J. clin. Microbiol.* **4**, 213–218.

Nichols, W. W., Dorrington, S. M., Slack, M. P. E. & Walmsley, H. L. 1988 Inhibition of tobramycin diffusion by binding to alginate. *Antimicro. Agents Chemo.* **32**, 518–523.

Peters, R., Peters, J., Tews, K. H. & Bahr, W. 1974 A microfluorimetric study of translational diffusion in erythrocyte membranes. *Biochem. biophys. Acta* **367**, 282–294.

Peters, R. & Scholz, M. 1991 Fluorescence Photobleaching Techniques. In *New techniques of optical microscopy and microspectroscopy* (ed. R. J. Cherry), pp. 199–228. London: Macmillan Press.

Rigler, R., Mets, U., Widengren, J. & Kask, P. 1993*a* Fluorescence correlation spectroscopy with high count rate and low background: analysis of translational diffusion. *Eur. Biophys. J.* **22**, 169–175.

Rigler, R., Widengren, J. & Mets, U. 1993*b* Interactions and kinetics of single molecules as observed by Fluorescence Correlation Spectroscopy. In *Fluorescence spectroscopy* (ed. O. S. Wolfbeis), pp. 13–23. Berlin: Springer.

Rueska, I., Robbins, J., Lashen, E. S. & Costerton, J. W. 1982 Biocide testing against corrosion-causing oil-field bacteria helps control plugging. *Oil Gas J.* March edn, pp. 253–264.

Russell, R. R. B. 1979 Glucan-binding proteins of *Streptococcus mutans* serotype c. *J. gen. Microbiol.* **112**, 197–201.

Sauer, H., Pratsch, L., Fritzsch, G., Bhakd, S. & Peters, R. 1991 Complement pore genesis observed in erythrocyte membranes by fluorescence microscopic single-channel recording. *Biochem. J.* **276**, 395–399.

Schäfer, F. 1989 Evaluation of the anticaries benefit of fluoride toothpastes using an enamel insert model. *Caries Res.* **23**, 81–86.

Staat, R. H., Langley, S. D. & Doyle, R. J. 1980 *Streptococcus mutans* adherence: presumptive evidence for protein-mediated attachment followed by glucan-dependent cellular accumulation. *Infect. Immun.* **27**, 675–681.

Sutton, N. A., Hughes, N. P. & Handley, P. S. 1994 A comparison of SEM techniques, low temperature SEM and the Electroscan wet SEM to study the structure of a biofilm of *Streptococcus crista* CR3. *J. appl. Bact.* **76**, 448–454.

Tatevossian. A. 1985 The effect of heat inactivation, tortuosity, extracellular polyglucan and ion exchange sites of the diffusion of ^{14}C-sucrose in human dental plaque residue *in vitro*. *Arch. Oral Biol.* **30**, 365–371.

Thomas, J. & Webb, W. W. 1990 Fluorescence photobleaching recovery: a probe of membrane dynamics. In *Noninvasive techniques in cell biology*, pp. 129–152. New York: Wiley-Liss Inc.

Torquato, S. & Kim, I. C. 1989 Efficient simulation technique to compute effective properties of heterogenous media. *Appl. Phys. Lett.* **55**, 1847–1849.

Widengren, J., Rigler, R. & Mets, U. 1994 Triplet-state monitoring by Fluorescence Correlation Spectroscopy. *J. Fluoresc.* **4**, 255–258.

Wolfaardt, G. M., Lawrence, J. R., Robarts, R. D., Caldwell, S. J. & Caldwell, D. E. 1994 Multicellular organisation in a degrative biofilm community. *Appl. Envir. Microbiol.* **60**, 434–446.

Wu-Yuan, C. D. & Gill, R. E. 1992 An 87 kilodalton glucan-binding protein of *Streptococcus sobrinus* B13. *Infect. Immun.* **60**, 5291–5293.

Received 6 March 1995; accepted 22 May 1995

PHILOSOPHICAL TRANSACTIONS OF THE ROYAL SOCIETY B BIOLOGICAL SCIENCES

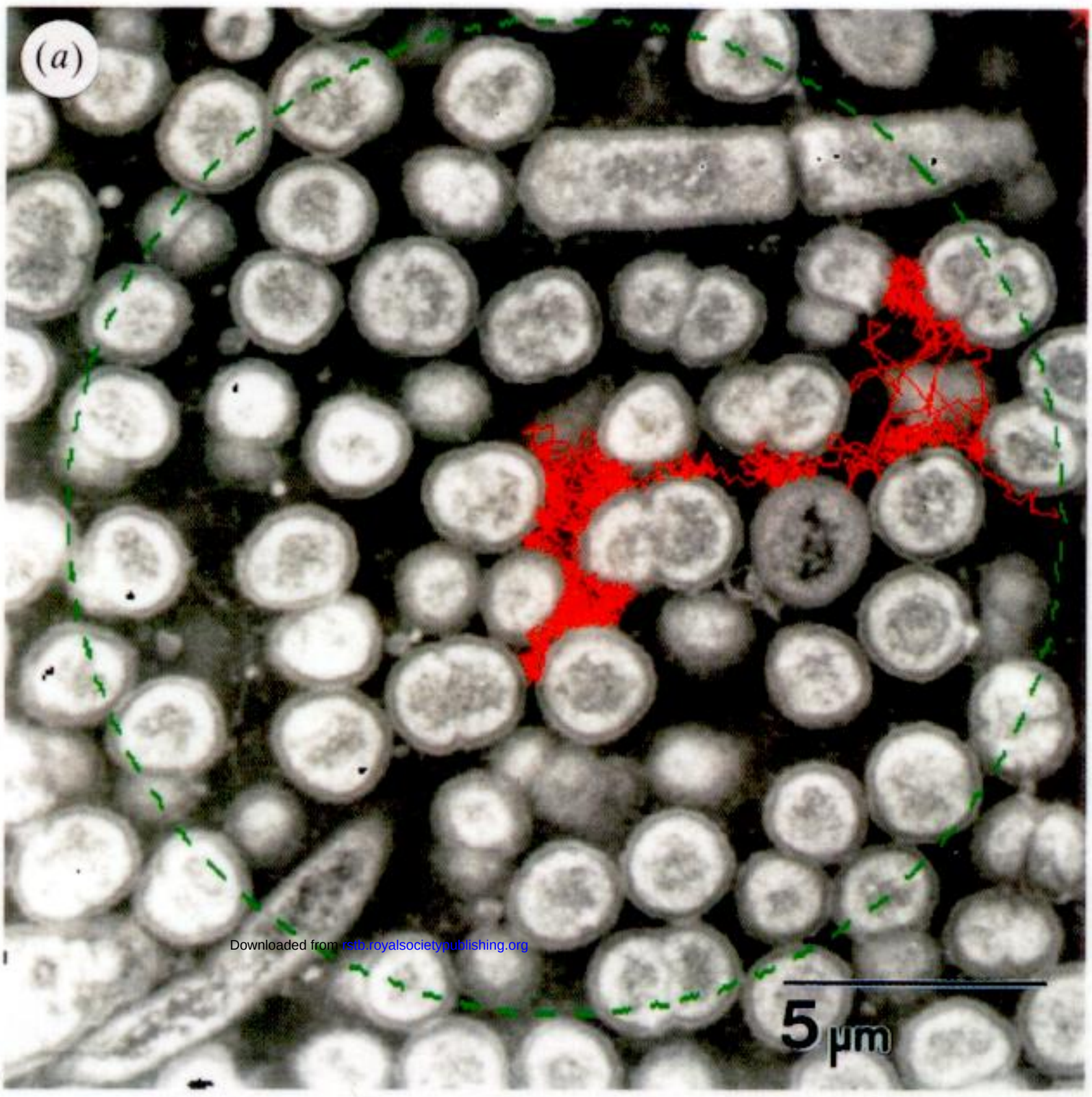

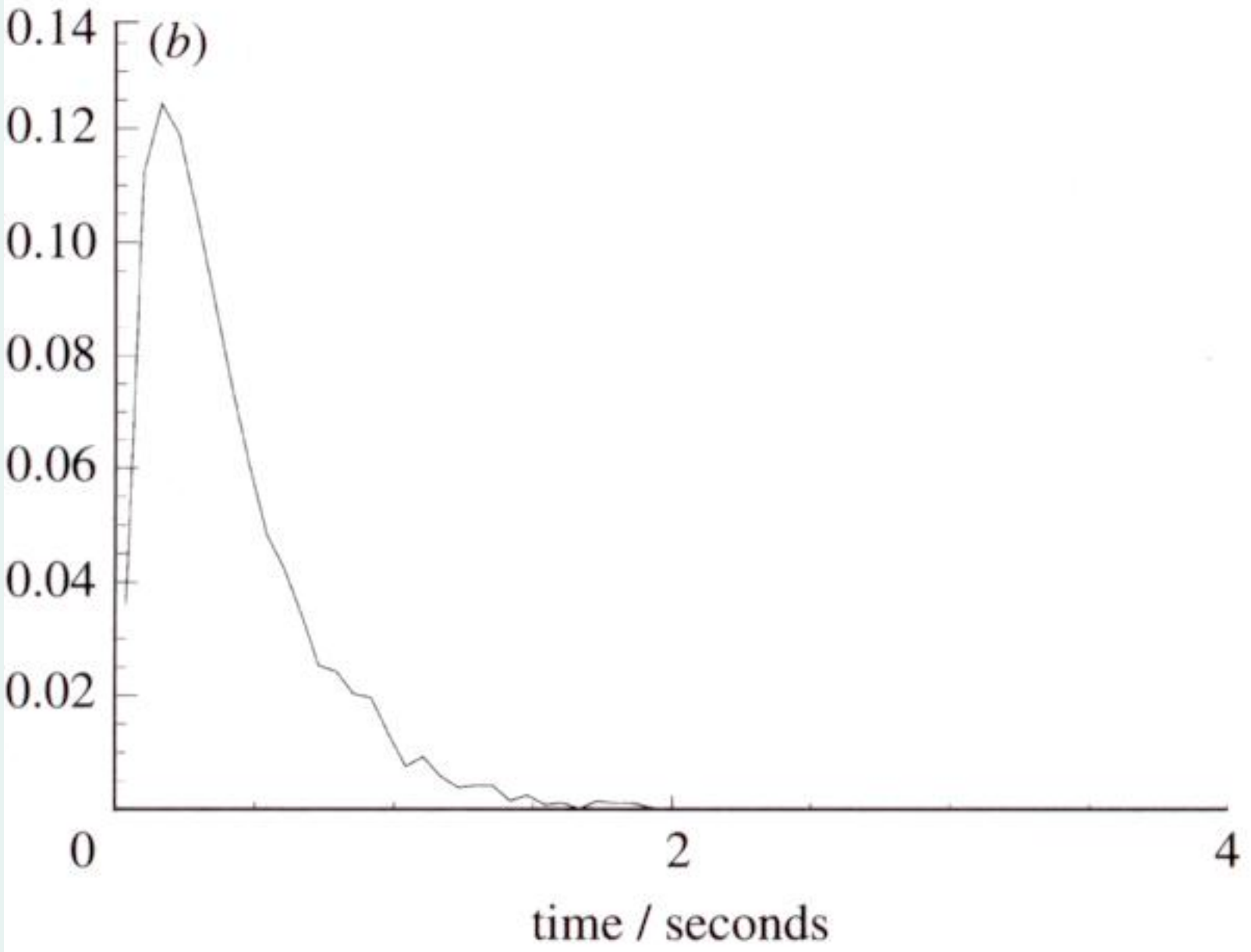

Figure 4. (*a*) Simulated random walk, with optimised step size, through a typical transmission electron microscopy image of a bacterial biofilm. Walk is shown in red and boundary of monitored area, L, is shown in green. (*b*) The distribution of passage times obtained from trajectories through the above microstructure (3000 walks, $D_0 = 10^{-6}\ \mathrm{cm^2\ s^{-1}}$).

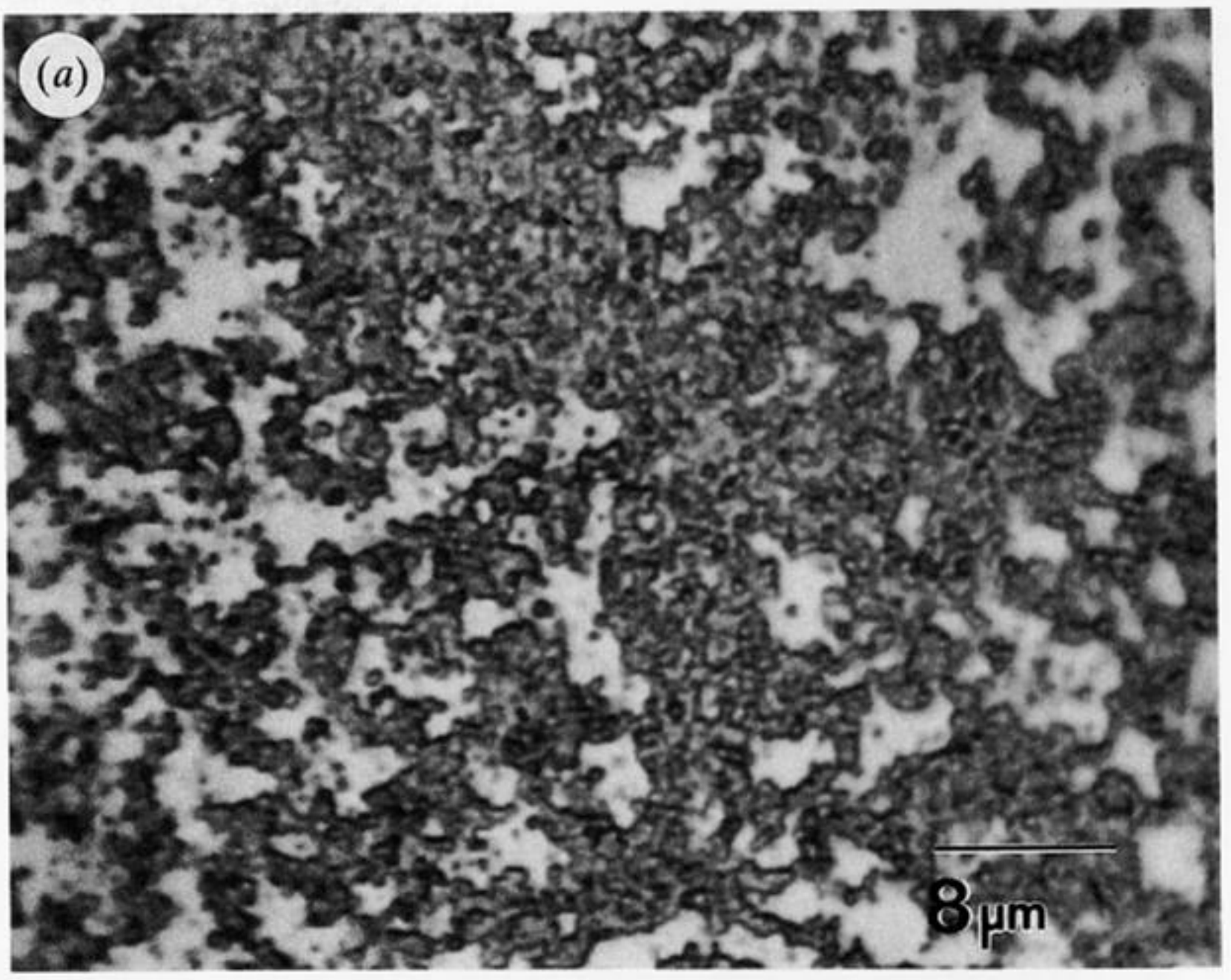

gure 8. Differential interference contrast optical micro-aphs of bacterial biofilms: (*a*) sucrose starved *in vitro* ofilm; (*b*) sucrose supplemented *in vitro* biofilm; and (*c*) *ex o* plaque.

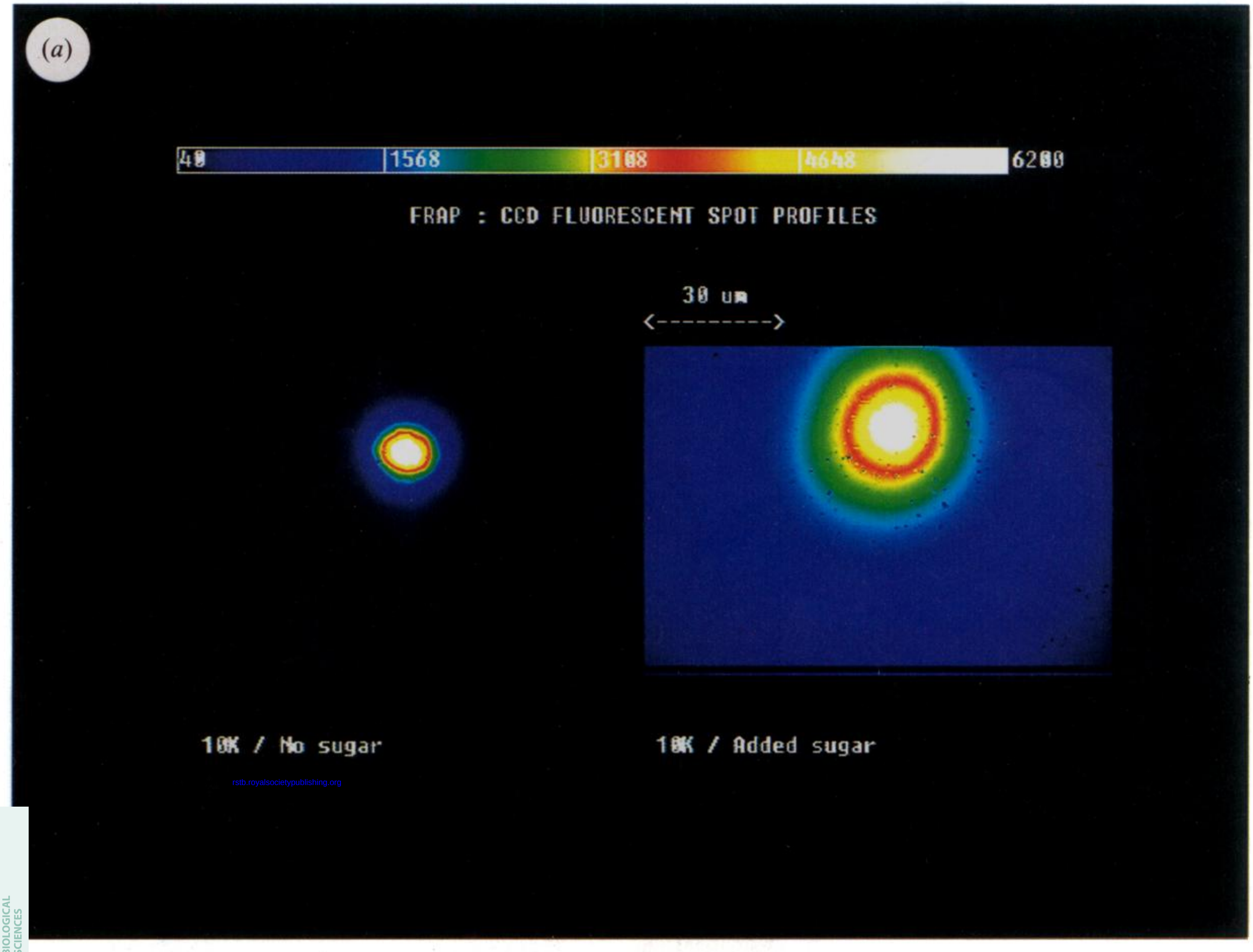

Figure 9. CCD Fluorescent spot images taken under non-bleaching conditions for 10 kDa dextran in either sucrose-starved (top-left) or sucrose supplemented (top-right) *in vitro* biofilms. Central horizontal sections through these images are shown in the bottom-left (non-sucrose) and bottom-right (sucrose supplemented) panels, along with nonlinear least-squares curvefits of the data to a gaussian profile and a quadratic background polynomial (dotted line).

PHILOSOPHICAL TRANSACTIONS OF THE ROYAL SOCIETY B BIOLOGICAL SCIENCES

igure 10. Low temperature scanning electron micrographs of sucrose supplemented *in vitro* biofilms: (*a*) low agnification, showing an open bacterial network; and (*b*) high magnification, showing the variety of bacterial orphologies and extracellular material.

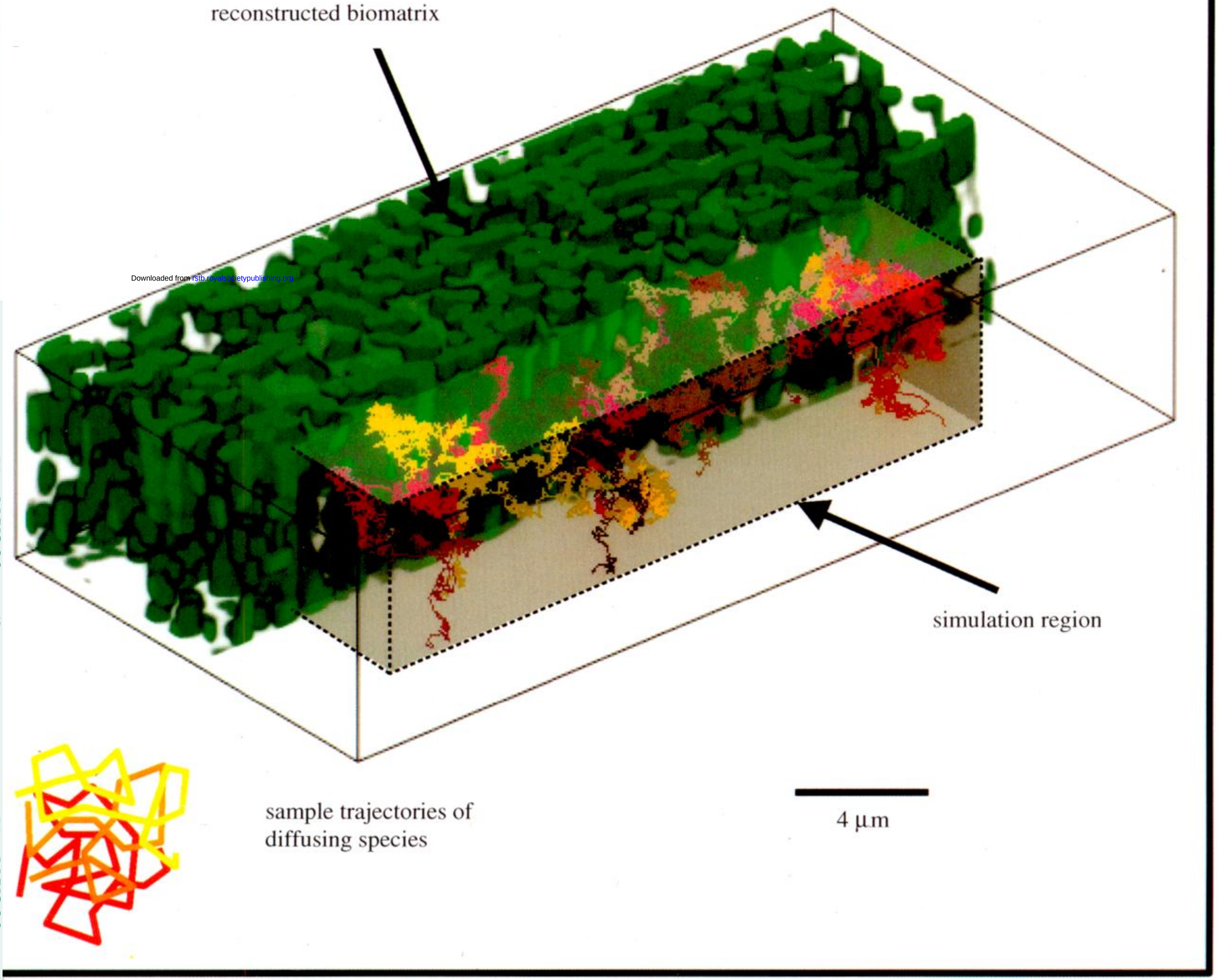

Figure 11. Random walks through a 3-D reconstructed biofilm, obtained from a set of confocal laser scanning microscopy images. Rendered biofilm microstructure is shown on the left (green). Walks, begun at the top surface of the biofilm, are shown on right (brown and red).